Genomic Deletions Correlate with Underexpression of Novel Candidate Genes at Six Loci in Pediatric Pilocytic Astrocytoma[1]

Nicola Potter[*], Aikaterini Karakoula[*], Kim P. Phipps[†], William Harkness[†], Richard Hayward[†], Dominic N. P. Thompson[†], Thomas S. Jacques[‡,§], Brian Harding[§], David G. T. Thomas[¶], Rodger W. Palmer[#], Jeremy Rees[*], John Darling[**] and Tracy J. Warr[*]

[*]Department of Molecular Neuroscience, Institute of Neurology, University College London, National Hospital for Neurology and Neurosurgery, London, WC1N 3BG, UK; [†]Department of Neurosurgery, Great Ormond Street Hospital for Children NHS Trust, London, WC1N 3JH, UK; [‡]Neural Development Unit, Institute of Child Health, University College London, London, WC1N 3JH, UK; [§]Department of Histopathology, Great Ormond Street Hospital for Children NHS Trust, London, WC1N 3JH, UK; [¶]National Hospital for Neurology and Neurosurgery, London, WC1N 3BG, UK; [#]North East London Regional Cytogenetics Laboratory, Great Ormond Street Hospital for Children NHS Trust, London, WC1N 3BG, UK; [**]Research Institute in Healthcare Science, School of Applied Sciences, University of Wolverhampton, Wolverhampton, WV1 1SB, UK

Abstract

The molecular pathogenesis of pediatric pilocytic astrocytoma (PA) is not well defined. Previous cytogenetic and molecular studies have not identified nonrandom genetic aberrations. To correlate differential gene expression and genomic copy number aberrations (CNAs) in PA, we have used Affymetrix GeneChip HG_U133A to generate gene expression profiles of 19 pediatric patients and the SpectralChip 2600 to investigate CNAs in 11 of these tumors. Hierarchical clustering according to expression profile similarity grouped tumors and controls separately. We identified 1844 genes that showed significant differential expression between tumor and normal controls, with a large number clearly influencing phosphatidylinositol and mitogen-activated protein kinase signaling in PA. Most CNAs identified in this study were single-clone alterations. However, a small region of loss involving up to seven adjacent clones at 7q11.23 was observed in seven tumors and correlated with the underexpression of *BCL7B*. Loss of four individual clones was also associated with reduced gene expression including *SH3GL2* at 9p21.2–p23, *BCL7A* (which shares 90% sequence homology with *BCL7B*) at 12q24.33, *DRD1IP* at 10q26.3, and *TUBG2* and *CNTNAP1* at 17q21.31. Moreover, the down-regulation of *FOXG1B* at 14q12 correlated with loss within the gene promoter region in most tumors. This is the first study to correlate differential gene expression with CNAs in PA.

Neoplasia (2008) 10, 757–772

Introduction

The most prevalent brain tumors in the pediatric population are astrocytomas, which most frequently manifest as pilocytic astrocytoma (PA), World Health Organization (WHO) grade I [1]. Pilocytic astrocytomas are commonly located in the cerebellum and can often be completely surgically resected, resulting in excellent long-term survival [2]. However, a small number of PA recur after resection and may occasionally undergo malignant transformation [3].

The genetic events that contribute to the development of PA are poorly defined. Cytogenetic analysis of pediatric PA has shown that most of these tumors (>70%) have a normal karyotype. Numerical and structural abnormalities of chromosomes 5, 6, 7, 8, and 9 have been reported, although definitive, nonrandom aberrations have not yet been identified [4–8]. Loss of the p53 locus on chromosome 17p has been reported in some PA studies but not consistently [9–11]. Similarly, although *TP53* gene mutations were found in 7 of 20 pediatric PA, other studies have failed to confirm these findings [12,13].

Global expression technology can now generate detailed gene expression profiles of tumors, and statistical algorithm–based classifications can be used to identify subgroups with clinical or biologic significance [14,15]. Array gene expression profiles of 21 pediatric PA have shown that genes involved in neurogenesis, cell adhesion, synaptic transmission, central nervous system development, potassium ion transport, protein dephosphorylation, and cell differentiation were significantly deregulated. The same study also demonstrated that the tumors clustered into two groups could be distinguished by the extent of myelin basic protein staining [16]. A similar approach has also been used to identify an expression signature that can stratify PA according to tumor location. A signature of 36 genes showed differential expression between supratentorial PA and those arising in the posterior fossa [17].

Array-based comparative genomic hybridization (aCGH) has recently been used to define genome-wide aberrations at a resolution of 1 Mb in adult malignant astrocytoma [18–24]. Only one previous study has used array technology to investigate chromosome copy number aberrations (CNAs) in PA [25]. Whole-chromosome aberrations were only observed in tumors arising in patients older than 10 years, in which the most common aberrations were gain of chromosomes 5 and 7, present in 13% and 17% of cases, respectively. Whole-chromosome aberrations of chromosome 15 were present in 6% of cases and of chromosomes 4, 6, 9, 10, 11, 12, and 20 in 3% of cases [25]. Single-nucleotide polymorphic allelic arrays have also been used to identify regions of allelic imbalance in low-grade pediatric gliomas including six PA. No detectable loss of heterozygosity was found at any of the 11,562 single-nucleotide polymorphic loci investigated in the PA [26]. It is also possible that epigenetic events such as aberrant promoter hypermethylation are common genomic alterations in pediatric low-grade astrocytoma and that they may have a greater impact on tumor development [27].

The aim of the present study was to correlate aberrant gene expression in pediatric PA with CNAs or gene promoter hypermethylation to identify and characterize cellular pathways that are involved in tumor development and growth. We have used the Affymetrix GeneChip HG_U133A (Affymetrix, Santa Clara, CA) to generate gene expression profiles and to identify aberrantly expressed genes in 19 pediatric PA biopsies. In 11 of 19 cases, we also identified CNAs using the aCGH SpectralChip 2600 (Spectral Genomics, Houston, TX). Both approaches were validated by real-time quantitative polymerase chain reaction (RT-QPCR). The methylation status of the promoter re-

gions of six genes, showing significant underexpression in the PA compared to the normal controls, was examined using methylation-specific PCR (MSP) and bisulfite sequencing to investigate alternative mechanisms of transcriptional silencing in PA. These genes have previously been reported as being methylated in astrocytoma or in other tumors or cancer [28–33].

Materials and Methods

Tumor Samples and RNA Preparation

Pilocytic astrocytoma tumor tissue was obtained with informed consent from 19 pediatric patients directly from the operating theater and was stored in liquid nitrogen until ready for use. All tumor samples were directly adjacent to tumor tissue processed for routine histologic evaluation and were first examined macroscopically to ensure that no frankly normal tissue was present. They were diagnosed according to the WHO classification and were reviewed by two neuropathologists [1]. The patients' mean age at diagnosis was 5.8 years (range, 1.75–11.5 years), with a female/male ratio of 8:11. At the time of this study, patient follow-up was available from diagnosis for 17 children who remain alive (follow-up ranged from 1 to 160 months from diagnosis; Table W1).

Total RNA was isolated from the 19 tumor samples using TRIzol reagent (Invitrogen Ltd, Paisley, UK) followed by cleanup using an RNeasy mini spin column (Qiagen, Crawley, UK). The quality and quantity of each sample were assessed using the Agilent 2100 Bioanalyser (Agilent Technologies Ltd, West Lothian, UK). Control RNA, consisting of four pooled normal whole-brain total RNA samples from young adults between 21 and 29 years of age, were obtained from AMS Biotechnology (Abingdon, Oxfordshire, UK) as previously described by Wong et al. [16].

cRNA Synthesis, Array Hybridization, and Array Scanning

Total RNA from 19 PA and 4 pooled normal whole-brain samples was used to prepare biotinylated target RNA following the manufacturer's instructions (Affymetrix). Briefly, 8 μg of total RNA was used to generate first-strand cDNA using a T7-linked oligo (dT) primer. Second-stand synthesis was then completed followed by a final transcription step with biotinylated UTP and CTP to label and amplify cRNA. The labeled cRNA was hybridized overnight to the HG_U133A array (Affymetrix). The arrays were washed and stained with streptavidin–phycoerythrin and were scanned using an Affymetrix GeneChip Scanner 3000. Array background, Q values, and mean intensities were within acceptable ranges for all arrays.

Affymetrix Array Data Analysis

Analysis was carried out using GeneSpring version 7.2 (Silicon Genetics, Redwood City, CA). The samples were analyzed in one experiment, and data transformation normalization was completed. Measurements less than 0.01 (set as a standard cutoff) were readjusted to 0.01, and per-chip normalizations were completed dividing all measurements on each array by the 50th percentile. The resulting expression levels were centered on 1 for each chip. The experiment was then normalized to the control samples (per gene normalization).

Identification of Aberrantly Expressed Genes

Data filters were applied after the raw expression data had been normalized, to remove unreliable and unnecessary data from further analysis including genes that were constant in both control and tumor

samples and Affymetrix standard control genes. Unsupervised hierarchical clustering with the remaining 10,653 informative probe sets was used to cluster the tumors according to gene expression profile similarity. A t test and Bonferroni multiple correction test ($P < .05$) were used to identify genes that showed a significant difference in expression between PA and normal controls. The variance statistic was derived from the multiple samples in each condition. A filter tool was then used to identify genes that showed a greater than twofold change in expression between the two conditions. From the 10,653 reliable expression results, 2273 probe sets that showed a significant and greater than twofold change in expression between PA and control samples, as described by Sowar et al. [34], were identified. These represented 1844 specific genes that were used for further analysis by Onto-Tools [35,36]. This software generates functional profiles of differentially expressed genes and assesses the impact of their alterations on biologic processes and pathways. The pathways used by Onto-Tools originate from the Kyoto Encyclopedia of Genes and Genomes (KEGG) database [37].

Validation of Differential Gene Expression by RT-QPCR Analysis

Real-time quantitative polymerase chain reaction analysis was completed for six genes that showed a twofold and significant difference in expression between PA and normal controls to validate the Affymetrix array results. RNA was available for RT-QPCR analysis from 16 of 19 tumors and 4 normal controls. cDNA was synthesized from 1 μg of total RNA using the QuantiTect Reverse Transcription Kit (Qiagen) following the manufacturer's instructions. Gene-specific oligonucleotide probes and primer pairs were obtained from Assays on Demand (Applied Biosystems, Warrington, UK) for *CCNA1*, *SPINT2*, *MAPK1*, *MATK*, *TIMP1*, and *MCL1*. All probes were designed across exon–exon boundaries. The TaqMan Universal PCR Master Mix No AmpErase UNG was used in a 25-μl reaction volume after cycling conditions recommended by the manufacturer. *β-Actin* was used as an endogenous control. All reactions were completed as single-well triplicates using the ABI Prism 7000 Sequence Detection System. No-template and no-amplification controls were included in each experiment. The comparative C_T method (PE Applied Biosystems, Warrington, UK) was used to determine the relative ratio of expression for each gene.

DNA Preparation and aCGH

Tumor tissue was available for aCGH analysis from 11 of 19 PA. Genomic DNA was isolated from the same tissue mass as total RNA using DNA Mini Kit following the manufacturer's instructions (Qiagen). Array-based comparative genomic hybridization was carried out using the SpectralChip 2600 following manufacturer's instructions (Spectral Genomics). The SpectralChip 2600 is a human BAC array that generates genome-wide molecular profiles at a resolution of 1 Mb allowing quantitative analysis. Each of the 2600 complementary BAC elements are printed on a glass slide, fluorescent-labeled normal and tumor DNA are cohybridized to the array, and dye ratios are calculated for each clone. Briefly, 1 μg of tumor and pooled sex-mismatched reference DNA (Promega, Southampton, UK) were differentially labeled with Cy5-dCTP or Cy3-dCTP using random prime labeling (Bioprime Labeling Kit; Invitrogen). Labeled tumor and reference DNA were cohybridized to the SpectralChip at 37°C for 16 hours in a hybridization chamber (Corning, Inc., Corning, NY). Arrays were washed at 50°C for 20 minutes in 50% formamide/2× SSC followed by 2× SSC/0.1% Tween 20 for 20 minutes and 0.2× SSC for 10 minutes. Arrays

were then washed in 80% ethanol and blown dry using nitrogen gas. Finally, the arrays were scanned using a microarray scanner (GenePix Personal 4100A; Molecular Devices, CA). Each experiment was duplicated swapping the dye labels between tumor and reference DNA.

Array-Based Comparative Genomic Hybridization Analysis

The scanned images were analyzed using GenePix Pro 6 software (Molecular Devices). Image spots were defined by an automatic grid feature that correlates the BAC clone position on the array with clone details including genomic locations. The spots were adjusted where necessary, and the dye intensities were calculated. Further analysis was completed using Formatter Software (Digital Scientific, Cambridge, UK; MIDAS Team) [38]. Preliminary analysis involved the removal of defective spots, that is, those without a signal, and background corrections were applied. A flip-dye consistency check involving the cross-log ratios of each signal from the duplicated clone spots on each array and from the dye swap experiment was also completed, and those signals that showed a greater than ±2SD variation between replicates were discarded [39,40].

Iterative linear regression global normalizations were completed for each sample reducing the SD of spot $\log_2$ ratios. In this approach, the SD of a given sample was continuously recalculated, removing outliers, until the correlation coefficients converged to a constant value. The final value is referred to as the modified SD (MSD). The outlier range used for this was ±2SD [41]. Those clones that showed a $\log_2$ ratio in excess of 3MSD were deemed as gained or lost. This approach assumes that data variations are random, and constant nonchanging results form most data. Theoretically, only 0.7% of data values will occur outside the threshold; therefore, any deviations exceeding 3SD are considered true positives [39,40].

Validation of DNA Copy Number by RT-QPCR Analysis

To validate the SpectralChip 2600 array experiments, RT-QPCR analysis to determine relative DNA copy number was completed at five genomic regions and/or gene loci including 1p36.32, 14q12, the promoter region of *FOXG1B* at 14q12, *BCL7B* at 7q11.23, and *BLC7A* at 12q24.33. Primer and oligonucleotide probe sets were designed within gene exon boundaries using primer design Web server and software packages (http://frodo.wi.mit.edu/cgi-bin/primer3/primer3_www.cgi) and Primer Express and were purchased from MWG-Biotech (Milton, Keynes, UK). *β-Actin*, at 7p12, was used as an endogenous control because this region was not altered in any of the PA in this study (see Table W2 for specific primer and probe sequences and concentrations). Probes for the genes of interest were labeled with the FAM fluorescent report, and the endogenous control probe was labeled with VIC. Sufficient DNA was available from 10 of 11 tumors investigated using the SpectralChip 2600 array and 4 additional tumors, for which expression array analysis had been completed (IN2356, IN2825, IN2921, and IN3156). DNA extracted from blood samples of four normal individuals and one pooled male and one pooled female DNA samples (Promega) were used as normal reference controls.

The RT-QPCR experiments were carried out using the ABI Prism 7000 Sequence Detection System. Reactions were completed as single-well triplicates in a final volume of 25 μl consisting of 1× QuantiTect Probe PCR Mix (Qiagen), probe and primers at the required concentrations, and 25 ng of genomic DNA. No-template and no-amplification controls were also included for each locus investigated. The thermal cycling profile consisted of a 15-minute heat activation step at 95°C, followed by 40 cycles at 95°C for 10 seconds and 60°C for 1 minute.

Before genomic quantification, primer limitation experiments were carried out to determine optimum primer concentrations for each experiment (see User Bulletin #2, Applied Biosystems, Warrington, UK). Primer concentrations that generated the highest magnitude of signal intensity (ΔRn) but lowest cycle threshold (C_T) at a given threshold were selected. The standard curve method (PE Applied Biosystems, Warrington, UK) was used to determine the relative copy number for each locus. A standard curve was included on each 96-well plate for control and target regions consisting of serially diluted normal genomic DNA (pooled blood from 20 healthy individuals). Only standard curves with correlation coefficients of 0.98 and higher were used for genomic copy number analysis. Tumors with values less than or equal to the copy number of controls minus the 95% reference range of controls (or 2× SD of controls) were considered to have genomic loss, whereas a value greater or equal to the copy number of controls plus 95% reference range of controls (or 2× SD of controls) was regarded as gain [42,43].

Methylation-Specific PCR and Sequencing

The methylation status of the promoter regions of six genes was investigated in 17 of 19 PA using MSP. Sequencing was used to confirm these results in two tumors and one normal brain control. The MSP and sequencing primer pairs for this study were either adapted or designed according to MSP principles [44,45] with the aid of the CpG island identification Web server (http://www.uscnorris.com/cpgislands2/), primer design Web server and software packages (http://frodo.wi.mit.edu/cgi-bin/primer3/primer3_www.cgi), and Primer Express (see Tables W3 and W4 for MSP and sequencing primer information).

After sodium bisulfite modification of tumor and normal DNA as described previously, MSP was carried out in a 25-µl volume with HotStart Taq (Qiagen) [44]. After an initial step of 95°C for 15 minutes, DNA was amplified by 35 cycles for 30 seconds at 95°C, for 30 seconds at the optimal annealing temperature for each primer pair, and for 30 seconds at 72°C, followed by a final extension step at 72°C for 5 minutes. Polymerase chain reaction analysis for sequencing was carried out in a 50-µl volume with HotStart Taq (Qiagen). After a 15-minute incubation at 95°C, DNA was amplified by 38 cycles at 94°C for 15 seconds, optimal annealing temperatures for primer pairs for 30 seconds and at 72°C for 45 seconds, followed by a final extension at 72°C for 5 minutes. A blank control containing all MSP components except the sample DNA and two positive controls (normal DNA and universally methylated DNA, both of which are bisulfite-treated as described previously) was included in each experiment. Products were separated using a 1.5% agarose gel containing ethidium bromide and 1× Tris-borate-EDTA buffer. The products were visualized by UV light.

Polymerase chain reaction amplifications of DNA for sequencing were performed using the BigDye Terminator v1.1 cycle sequencing kit following manufacturer's instructions (Applied Biosystems, Foster City, CA). Sequencing was carried out using an ABI 3730×1 DNA Analyser, and raw data were analyzed with SeqScape software v2.5 (Applied Biosystems, Foster City, CA).

Results

Gene Expression Profiles of Pediatric PA

Using the Affymetrix GeneChip HG_U133A, we have studied the expression pattern of approximately 22,000 genes in pediatric PA compared to normal brain (see Table W5 for all Affymetrix GeneChip raw data). Unsupervised hierarchical clustering using 10,653 reliable gene expression results was used to generate a dendrogram illustrating the similarity in expression profiles of the 19 PA (Figure 1). The tumor and normal control samples clustered independently. However, the PA did not group or order according to patient age, sex, or tumor location, and no consistent expression profiles could be associated with these clinical parameters or patient outcome. Moreover, no further subgroups were clearly defined, in contrast to the previous findings [16,17]. Wong et al. [16] described a molecular signature of 89 genes that distinguished two subgroups of PA representing tumors with different potentials of progression. A list of the 89 genes was not available in the literature. However, 16 of these 89 genes were described by Wong et al. [16] and were involved in biologic processes that significantly altered between the two subgroups. In total, 13 of these 16 genes showed reliable data in the present study and were used to cluster the 19 PA. The tumors did not cluster into subgroups, and a continuous increase or decrease in the expression of these 13 genes was seen between tumors that are least similar (Figure W1, a and b).
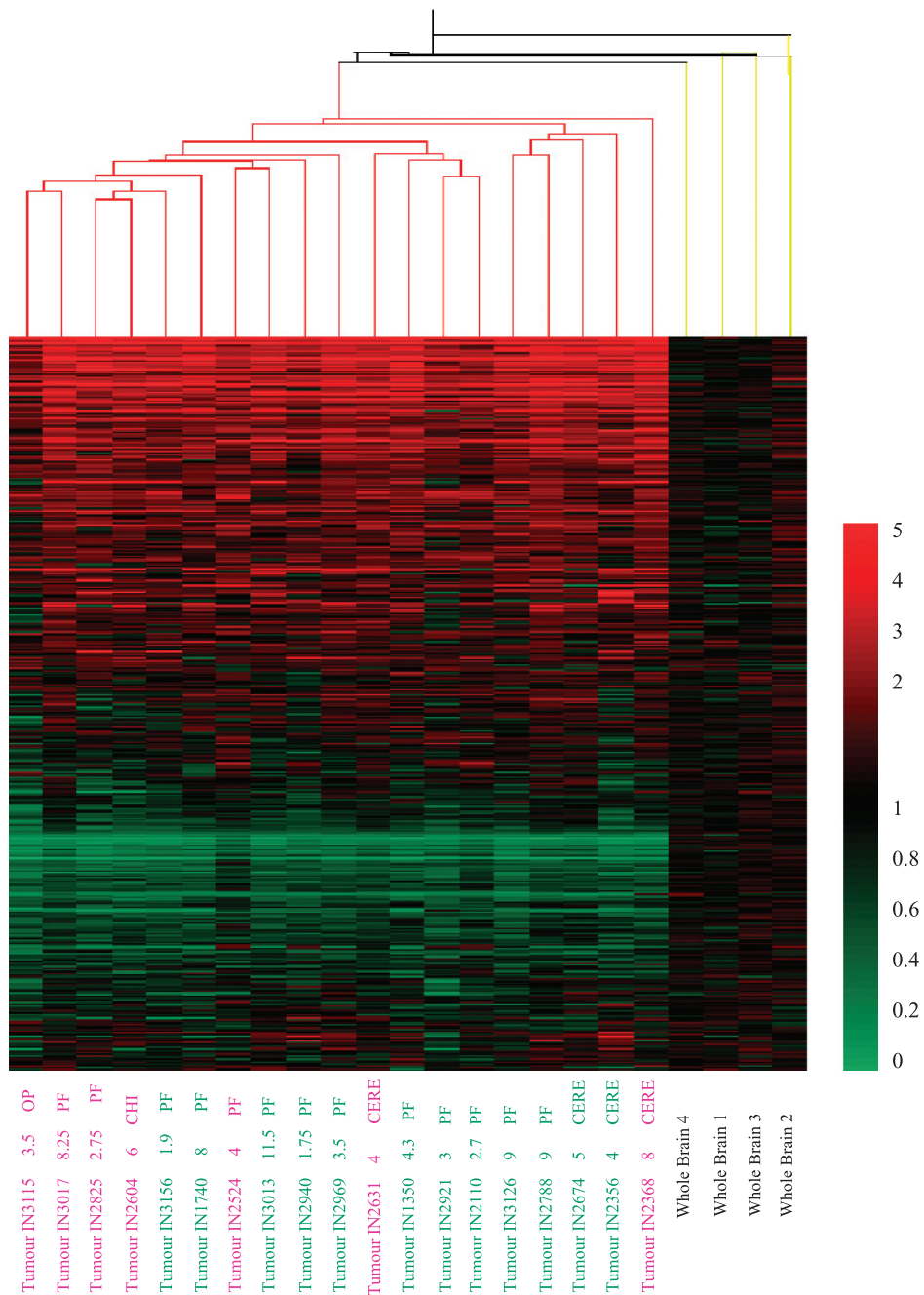
From 10,653 reliable expression results, 1844 genes showed a two-fold and significant change in expression in PA compared to the normal controls. Of these, 1002 were up-regulated and 842 were down-regulated. Genes that showed a greater than 10-fold change in expression and were either involved in a KEGG pathway or have been well characterized were investigated further (Table 1). *SERPINA3*, a protease inhibitor, showed the largest up-regulation in gene expression with an 80.89-fold change in the tumors compared to normal brain. *FOXG1B*, a member of the forkhead family of transcription factors, showed the largest down-regulation in gene expression with a 325.73-fold change.

The Onto-Tools software was used to rank the KEGG pathways influenced by the 1844 differentially expressed genes according to the extent of differential gene expression. Of the 53 pathways that were ranked, only those of interest are displayed in Table 2 (see Table W6 for all pathways involved in this analysis). The pathway most affected by differential gene expression (rank 1) was antigen processing and presentation, in which most genes are significantly up-regulated and located at 6p21.3.

To investigate if particular differentially expressed genes could influence several pathways and have an overall impact on tumor development, those genes involved in five or more pathways were identified (Table 3). Although *MAPK1* is involved in 17 pathways, this gene only showed a 2.01-fold down-regulation in expression. In contrast, genes with the largest fold changes are involved in fewer pathways. Only two genes, *CAMK2A* and *PRKCB1*, showed a greater than 10-fold change in expression and are involved in more than five pathways (Tables 1 and 3), suggesting that those genes with the highest degree of disregulation in pediatric PA may not have the greatest impact on cellular pathways.

Validation of Differential Gene Expression by RT-QPCR Analysis

To validate the expression results obtained from the Affymetrix array experiments, the expression of six genes that showed a two-fold and significant difference in expression in PA compared to the normal controls was assessed using RT-QPCR. The array data demonstrated that *CCNA1*, *SPINT2*, *MAPK1*, and *MATK* were

Figure 1. Unsupervised hierarchical clustering of 19 pediatric PA and 4 normal brain controls using 10,653 reliable gene expression results. The dendrogram color saturation is proportional to the magnitude of the difference from the mean, ranging from red (over-expressed) to green (underexpressed). Patient ages are in years at diagnosis. Tumor labels in green indicate a male patient, and pink a female patient. *CERE* indicates cerebellum; *CHI*, chiasmatic; *OP*, optic pathway; *PF*, posterior fossa.

significantly down-regulated and *TIMP1* and *MCL1* were significantly up-regulated. Real-time quantitative polymerase chain reaction confirmed these changes in gene expression in PA compared to normal brain (Table W7).

Genomic Aberrations Found in Pediatric PA

Array-based comparative genomic hybridization was carried out using the SpectralChip 2600 to identify regions of chromosome gain and loss in 11 pediatric PA. The array profile from the most altered

tumor, IN2368, is illustrated in Figure 2. In total, 97 individual BAC clones were found to be either gained or lost in one or more tumors. Of these, 26 were gained, 64 were lost, and 7 were either gained or lost in different tumors (Figure 3; see Table W8, *a–l*, for details of these 97 altered clones and the combined dye swap raw data for each sample). Several chromosome regions were frequently altered in PA. BAC clones mapping to 1p36.32, 14q12, 19p13.2, and 22q13.33 showed gain, loss, or both in 91%, 82%, 64%, and 91% of tumors, respectively. Other regions less frequently altered included the following: 7q11.2 and 8q21 in 45% of tumors; 7q34, 8q24.3, 10q21.3,

Table 1. Differentially Expressed Genes That Show a 10-Fold Minimum Change in Expression from the Normal and Are Involved in Specific Pathways or Are Well Characterized with Functions That Can Be Linked to Tumor Development.

Rank	Gene Symbol	Gene Description	Fold Change in Expression	Chromosome Location
1	SERPINA3	Serine (or cysteine) proteinase inhibitor, clade A (alpha-1 antiproteinase, antitrypsin), member 3	80.89	14q32.1
2	CHI3L1	Chitinase 3-like 1 (cartilage glycoprotein-39)	56.98	1q32.1
4	CHAD **2** (4, 11)	Chondroadherin	43.68	17q21.33
6	TIMP4	Tissue inhibitor of metalloproteinase 4	41.47	3p25
7	WEE1 **1** (38)	WEE1 homolog (Schizosaccharomyces pombe)	41.03	11p15.3–p15.1
11	T1A-2	Lung type-I cell membrane–associated glycoprotein	35.21	1p36
12	ABCC3	ATP-binding cassette, subfamily C (CFTR/MRP), member 3	33.72	17q22
15	IL1RAP **2** (1, 47)	Interleukin 1 receptor accessory protein	26.58	3q28
17	CSPG4	Chondroitin sulfate proteoglycan 4 (melanoma-associated)	23.77	15q23
19	AGTRL1 **1** (32)	Angiotensin II receptor–like 1	22.36	11q12
22	CD44	Homo sapiens CD44 isoform RC (CD44) mRNA, complete cds	19.88	11p13
24	MYT1	Myelin transcription factor 1	18.49	20q13.33
26	TAZ	Transcriptional coactivator with PDZ-binding motif (TAZ)	17.53	3q23–q24
31	TIMP1	Tissue inhibitor of metalloproteinase 1 (erythroid potentiating activity, collagenase inhibitor)	16.23	Xp11.3–p11.23
32	HLA-DPA1 **3** (1, 2, 32)	Major histocompatibility complex, class II, DP alpha 1	15.79	6p21.3
36	S100A10	S100 calcium binding protein A10 (annexin II ligand, calpactin I, light polypeptide (p11))	15.27	1q21
38	TLR2 **1** (14)	Toll-like receptor 2	14.66	4q32
40	TFPI **1** (12)	ESTs, weakly similar to cytokine receptor-like factor 2; cytokine receptor CRL2 precusor (Homo sapiens)	14.09	2q32
44	POSTN	Osteoblast-specific factor 2 (fasciclin I-like)	12.60	13q13.1
46	CHI3L2	Chitinase 3-like 2	12.22	1p13.3
48	CCL3	Chemokine (C–C motif) ligand 3	11.89	17q11–q21
49	MSR1	Macrophage scavenger receptor 1	11.87	8p22
50	SRPX	Sushi-repeat–containing protein, X chromosome	11.29	Xp21.1
51	CSPG2 **1** (2)	Chondroitin sulfate proteoglycan 2 (versican)	10.86	5q14.3
56	CD151	CD151 antigen	10.61	11p15.5
−74	FGF13 **2** (5, 6)	Fibroblast growth factor 13	−10.34	Xq26.3
−72	MEF2C **1** (5)	MADS box transcription enhancer factor 2, polypeptide C (myocyte enhancer factor 2C)	−10.48	5q14
−70	WNT10B **2** (28, 46)	wingless-type MMTV integration site family, member 10B	−10.50	12q13
−69	NPY1R **1** (32)	Neuropeptide Y receptor Y1	−10.96	4q31.3–q32
−67	ATP2B2 **1** (19)	Homo sapiens, similar to nuclear localization signals binding protein 1, clone IMAGE:4933343, mRNA	−11.22	3p25.3
−66	PRKCB1 **15** (3–5, 7, 8, 10, 16–19, 22, 28, 36, 39, 41)	Protein kinase C, beta 1	−11.24	16p11.2
−65	MAL	mal, T-cell differentiation protein	−11.55	2cen-q13
−62	CACNA2D3 **1** (5)	Calcium channel, voltage-dependent, alpha 2/delta 3 subunit	−11.89	3p21.1
−60	GRIN1 **3** (7, 19, 32)	Glutamate receptor, ionotropic, N-methyl D-aspartate 1	−12.15	9q34.3
−59	HTR2A **3** (10, 19, 32)	5-Hydroxytryptamine (serotonin) receptor 2A	−12.22	13q14–q21
−55	SNAP25 **1** (43)	Synaptosomal-associated protein, 25 kDa	−13.04	20p12–p11.2
−54	PTK2B **4** (8, 16, 17, 19)	PTK2B protein tyrosine kinase 2 beta	−13.42	8p21.1
−52	VIP **1** (32)	Vasoactive intestinal peptide	−14.27	6q26–q27
−50	VAMP1 **1** (43)	Vesicle-associated membrane protein 1 (synaptobrevin 1)	−15.17	12p
−48	NPY **2** (32, 35)	Neuropeptide Y	−15.63	7p15.1
−45	ENPP2	Ectonucleotide pyrophosphatase/phosphodiesterase 2 (autotaxin)	−17.09	8q24.1
−44	MBP	Myelin basic protein	−17.48	18q23
−39	HTR2C **3** (10, 1, 32)	5-Hydroxytryptamine (serotonin) receptor 2C	−19.23	Xq24
−37	P2RX5 **2** (19, 23)	Purinergic receptor P2X, ligand-gated ion channel, 5	−19.57	17p13
−32	MATK **2** (6, 15)	Megakaryocyte-associated tyrosine kinase	−23.75	19p13.3
−31	CRH **2** (22, 32)	Corticotropin-releasing hormone	−24.27	8q13
−22	NEFH **2** (25, 31)	Neurofilament, heavy polypeptide 200 kDa	−27.40	22q12.2
−21	ICAM5	Intercellular adhesion molecule 5, telencephalin	−27.70	19p13.2
−19	EGR4	Early growth response 4	−28.90	2p13
−15	CAMK2A **5** (7, 8, 19, 20, 28)	Calcium/calmodulin–dependent protein kinase (CaM kinase) II alpha	−36.76	5q33.1
−13	ATP2B2 **1** (19)	ATPase, Ca^{2+} transporting, plasma membrane 2	−39.22	3p26–p25
−11	SST **1** (32)	Somatostatin	−43.86	3q28
−10	ITPKA **2** (3, 19)	Inositol 1,4,5-trisphosphate 3-kinase A	−49.50	15q14–q21
−6	GABRA5 **1** (32)	γ-Aminobutyric acid (GABA) A receptor, alpha 5	−101.01	15q11.2–q12
−3	CACNG3 **1** (5)	Calcium channel, voltage-dependent, gamma subunit 3	−136.99	16p12–p13.1
−2	CCK **1** (32)	Cholecystokinin	−146.63	3q22–p21.3
−1	FOXG1B	Forkhead box G1B	−325.73	14q12–q13

The number of pathways that each gene is involved in is given in bold after the gene symbol. The numbers inside the parentheses correspond to the specific pathways in Table 2. Genes highlighted in red are involved in multiple pathways listed in Table 3.

and 17q21 in 36% of tumors; and 6q12, 6q13, 17q21.3, and 19p13.3 in 27% of tumors. A small region containing two adjacent clones at 1p13 was lost in one tumor and a region that varied in size containing up to seven adjacent clones at 7q11.23 was lost in seven tumors. Large-scale copy number variants (LCVs) in specific chromosome regions have been characterized in the normal population. Of 97 clones altered in PA of this study, 37 are located in regions of known LCV (Figure 3).

Validation of DNA Copy Number by RT-QPCR Analysis

To validate the results obtained from the SpectralChip 2600 array, RT-QPCR analysis was used to determine the relative genomic copy number at five genomic regions and/or gene loci (see Table W9 for standard curve method raw data). This approach confirmed CNAs (both loss and gain) of the BAC clone RP4-703E10 at 1p36.32 in 80% of cases (Tables 4 and 5). Loss of *BLC7A* at 12q24.33 was verified by RT-QPCR in the single tumor, which demonstrated loss of the equivalent BAC clone (RP11-87C12), and in 11 additional tumors, indicating the superior sensitivity of RT-QPCR analysis in the detection of small CNAs [46]. *BCL7B* lies within a small deletion of up to seven adjacent clones at 7q11.23. Real-time quantitative polymerase chain reaction analysis confirmed loss of this gene in five of six tumors and detected loss in seven additional cases. Loss of clone RP11-125A5 in the region of LCV at 14q12 was verified by RT-QPCR analysis in only two of eight tumors demonstrating loss by BAC array analysis, similar to the findings of the recent study by Qiao et al. [47].

Correlation of Genomic and Expression Array Data

Reliable gene expression data were not available for all genes located in the same regions as the 97 BAC clones which were lost and/or gained. Overall, loss of four single clones correlated with down-regulation of genes mapping to the same region. These comprised *SH3GL2* at 9p21.2–p23 (clone lost in one tumor), *DRD1IP* at 10q26.3 (clone lost in one tumor), *BCL7A* at 12q24.33 (clone lost in one tumor), and *TUBG2* and *CNTNAP1* at 17q21.31 (clone lost in two tumors). In seven tumors, there was also loss of a region at 7q11.23 containing up to seven adjacent clones that mapped to 71,658,093–73,945,118 (Figure 4). This region contains 47 genes in total, but only 17 were present on the Affymetrix GeneChip HG_U133A. Of these genes, seven showed unreliable expression data, nine were expressed at a normal level, and *BCL7B* was significantly down-regulated in all tumors compared to normal controls ($P < .05$). In addition, *FOXG1B* maps adjacent to the clone RP11-125A5 at 14q12, which was determined to be lost by aCGH and showed significant down-regulation in all PA compared to normal controls ($P < .01$). Real-time quantitative polymerase chain reaction analysis of relative DNA copy number of the *FOXG1B* promoter demonstrated genomic loss in 8 of 14 tumors.

Critically, although clone loss at these regions was not seen in every tumor, all samples showed a twofold and significant down-regulation in the specific genes at these loci listed in Table 6. No correlations were found between clone gain and gene overexpression.

Methylation-Specific PCR and Sequencing

Methylation-specific PCR products were only generated by primer sets specific for unmethylated promoter regions, indicating that the promoter regions of *CDKN1C*, *PRDM2*, *SPINT2*, *REPRIMO*, *CCNA1*, and *DAPK1* were not methylated in the 17 PA analyzed. Sequencing of each gene in IN3115 and IN2940 and normal brain confirmed that promoter region methylation was not present in either PA or

Table 2. The Pathway Express Results Ranking the KEGG Pathways Incorporating the 1844 Differentially Expressed Genes in PA.

| Rank	Unique Pathway ID	KEGG Database Pathway Name	Impact Factor	Genes in Pathway	Pathway Genes in Input (%)
1	1:04612	Antigen processing and presentation	76.6	86	24.4
2	1:04514	Cell adhesion molecules (CAMs)	24.1	132	25.8
3	1:04070	Phosphatidylinositol signaling system	23.2	79	27.8
4	1:04510	Focal adhesion	14.7	194	25.8
5	1:04010	MAPK signaling pathway	14.3	273	22.7
6	1:04810	Regulation of actin cytoskeleton	12.9	206	23.3
9	1:04210	Apoptosis	9.3	84	27.4
10	1:04540	Gap junction	9.3	99	25.3
11	1:04512	ECM–receptor interaction	9.1	87	26.4
12	1:04610	Complement and coagulation cascades	8.8	69	27.5
14	1:04620	Toll-like receptor signaling pathway	8.1	91	25.3
16	1:04670	Leukocyte transendothelial migration	7.8	117	23.1
17	1:04650	Natural killer cell mediated cytotoxicity	7.3	128	21.1
18	1:04662	B-cell receptor signaling pathway	7.2	63	27.0
19	1:04020	Calcium signaling pathway	7.0	176	18.2
24	1:04910	Insulin signaling pathway	5.7	135	20.7
25	1:01510	Neurodegenerative disorders	5.7	35	28.6
26	1:05210	Colorectal cancer	5.6	77	23.4
28	1:04310	Wnt signaling pathway	5.5	147	18.4
32	1:04080	Neuroactive ligand–receptor interaction	4.7	302	11.3
33	1:04660	T cell receptor signaling pathway	4.4	93	20.4
35	1:04920	Adipocytokine signaling pathway	4.0	69	20.3
36	1:04530	Tight junction	3.9	119	16.8
37	1:04520	Adherens junction	3.8	77	20.8
38	1:04110	Cell cycle	3.5	112	16.1
39	1:04370	Vascular endothelial growth factor (VEGF) signaling pathway	3.0	72	16.7
42	1:04150	mTOR signaling pathway	2.6	49	18.4
43	1:04130	SNARE interactions in vesicular transport	2.5	36	13.9
44	1:04350	TGFβ signaling pathway	2.3	84	15.5
45	1:04630	Jak–STAT signaling pathway	2.2	153	13.7
46	1:04340	Hedgehog signaling pathway	1.6	57	12.3
47	1:04060	Cytokine–cytokine receptor interaction	1.6	256	11.7
51	1:04140	Regulation of autophagy	0.8	29	3.4
52	1:04330	Notch signaling pathway	0.8	46	8.7

The pathways are ranked according to impact factor, taking into account the fold change, the number of genes disrupted in a pathway, and the influence each gene exerts on a pathway.

Table 3. The Pathway Express Results of Differentially Expressed Genes Involved in ≥5 Pathways.

Gene Symbol	Gene Description	Fold Change in Expression	Number of Pathways Gene Involved in	Chromosome Location
MAPK1	Mitogen-activated protein kinase 1	−2.01	**17** (4–8, 10, 17, 21, 22, 24, 26, 37, 39–42, 44)	22q11.21
PIK3CB	Phosphoinositide-3-kinase, catalytic, beta polypeptide	−2.05	**16** (3, 4, 6, 9, 14, 16–18, 24, 26, 33, 39–42, 45)	3q22.3
PIK3R1	Phosphoinositide-3-kinase, regulatory subunit 1 (p85 alpha)	−2.13	**16** (3, 4, 6, 9, 14, 16–18, 24, 26, 33, 39–42, 45)	5q13.1
PRKCB1	Protein kinase C, beta 1	−11.24	**15** (3–5, 7, 8, 10, 16–19, 22, 28, 36, 39, 41)	16p11.2
AKT3	v-akt murine thymoma viral oncogene homolog 3 (protein kinase B, gamma)	−2.54	**14** (4, 5, 9, 14, 18, 24, 26, 33, 35, 36, 39, 41, 42, 45)	1q43–q44
MAP2K1	Mitogen-activated protein kinase kinase 1	−4.17	**12** (4–8, 10, 17, 22, 24, 26, 39, 41)	15q22.1–q22.33
MAPK9	Mitogen-activated protein kinase 9	−3.48	**11** (4, 5, 8, 14, 15, 24, 26, 28, 35, 40, 41)	5q35
MAPK10	Mitogen-activated protein kinase 10	−2.28	**11** (4, 5, 8, 14, 15, 24, 26, 28, 35, 40, 41)	4q22.1–q23
PRKACB	Protein kinase, cAMP-dependent, catalytic, beta	−2.55	**11** (5, 7–10, 19, 20, 24, 28, 46, 48)	1p36.1
PPP3CA	Protein phosphatase 3 (formerly 2B), catalytic subunit, alpha isoform (calcineurin A alpha)	−4.13	**11** (5, 7, 9, 17–19, 21, 28, 31, 33, 39)	4q21–q24
PPP3CB	Protein phosphatase 3 (formerly 2B), catalytic subunit, beta isoform (calcineurin A beta)	−3.65	**10** (5, 7, 9, 17–19, 21, 28, 31, 33, 39)	10q21–q22
PRKX	Protein kinase, X-linked	2.08	**10** (5, 7, 8, 10, 19, 20, 24, 28, 46, 48)	Xp22.3
PPP3R1	Protein phosphatase 3 (formerly 2B), regulatory subunit B, 19 kDa, alpha isoform (calcineurin B, type I)	−3.05	**10** (5, 7, 9, 17–19, 21, 28, 33, 39)	2p15
IKBKB	Inhibitor of kappa light polypeptide gene enhancer in B cells, kinase beta	2.75	**9** (5, 9, 14, 15, 18, 24, 33, 35, 40)	8p11.2
JUN	v-jun sarcoma virus 17 oncogene homolog (avian)	2.49	**9** (4, 5, 8, 14, 15, 18, 26, 28, 33)	1p32–p31
PAK1	p21/Cdc42/Rac1–activated kinase 1 (STE20 homolog, yeast)	−7.87	**7** (4–6, 15, 17, 21, 33)	11q13–q14
TP53	Tumor protein p53 (Li-Fraumeni syndrome)	3.14	**7** (5, 9, 26, 28, 29, 31, 38)	17p13.1
PLCB1	Phospholipase C, beta 1 (phosphoinositide-specific)	−2.73	**7** (3, 7, 8, , 10, 19, 22, 28)	20p12
CALM1	Calmodulin 1 (phosphorylase kinase, delta)	−2.22	**7** (3, 7, 8, 19, 20, 24, 29)	14q24–q31
PDGFRA	Platelet-derived growth factor receptor, alpha polypeptide	5.76	**7** (4–6, 10, 19, 26, 47)	4q11–q13
CALM3	Calmodulin 3 (phosphorylase kinase, delta)	−2.31	**7** (3, 7, 8, 19, 20, 24, 29)	19q13.2–q13.3
ITGB1	Integrin, beta 1 (fibronectin receptor, beta polypeptide, antigen CD29 includes MDF2, MSK12)	2.26	**6** (2, 4, 6, 11, 16, 21)	10p11.2
ITPR1	Inositol 1,4,5-triphosphate receptor, type 1	−8.62	**6** (3, 7, 8, 10, 19, 22)	3p26–p25
ITPR2	Inositol 1,4,5-triphosphate receptor, type 2	5.42	**6** (3, 7, 8, 10, 19, 22)	12p11
ROCK1	Rho-associated, coiled-coil containing protein kinase 1	2.42	**6** (4, 6, 16, 21, 28, 44)	18q11.1
NFKBIA	Nuclear factor of kappa light polypeptide gene enhancer in B-cells inhibitor, alpha	2.17	**6** (9, 14, 15, 18, 33, 35)	14q13
ROCK2	Rho-associated, coiled-coil containing protein kinase 2	−2.40	**6** (4, 6, 16, 21, 28, 44)	2p24
CCND1	Cyclin D1	3.77	**5** (4, 26, 28, 38, 45)	11q13
CAMK2A	Calcium/calmodulin–dependent protein kinase (CaM kinase) II alpha	−36.77	**5** (7, 8, 19, 20, 28)	5q33.1
CAMK2B	Calcium/calmodulin–dependent protein kinase (CaM kinase) II beta	−8.77	**5** (7, 8, 19, 20, 28)	7p14.3–p14.1
GNAI3	Guanine nucleotide binding protein (G protein), alpha inhibiting activity polypeptide 3	2.72	**5** (10, 16, 21, 22, 36)	3p21
TGFB1	Transforming growth factor, beta 1 (Camurati–Engelmann disease)	2.32	**5** (5, 26, 38, 44, 47)	19q13.1
ACTN1	Actinin, alpha 1	2.26	**5** (4, 6, 16, 36, 37)	14q22–q24
PAK2	p21 (CDKN1A)–activated kinase 2	2.23	**5** (4–6, 21, 33)	3q29
FOS	v-fos FBJ murine osteosarcoma viral oncogene homolog	5.10	**5** (5, 14, 18, 26, 33)	14q24.3
ACTN2	Actinin, alpha 2	−2.52	**5** (4, 6, 16, 36, 37)	1q42–q43
MAP2K4	Mitogen-activated protein kinase kinase 4	−3.30	**5** (5, 8, 14, 15, 41)	17p11.2
PLA2G6	Phospholipase A2, group VI (cytosolic, calcium-independent)	−2.02	**5** (5, 8, 2, 39, 41)	22q13.1
PTPN6	Protein tyrosine phosphatase, nonreceptor type 6	2.21	**5** (17, 18, 33, 37, 45)	12p13
FAS	Fas (TNF receptor superfamily, member 6)	5.90	**5** (5, 9, 13, 17, 47)	10q24.1
CCND2	Cyclin D2	2.02	**5** (4, 26, 28, 38, 45)	12p13
PLA2G12A	Phospholipase A2, group XIIA	3.99	**5** (5, 8, 22, 39, 41)	4q25
GNAS	GNAS complex locus	−4.93	**5** (8, 10, 19, 22, 48)	20q13.3
GNAI1	Guanine nucleotide binding protein (G protein), alpha inhibiting activity polypeptide 1	−2.25	**5** (10, 16, 21, 22, 36)	7q21
CAMK2G	Calcium/calmodulin–dependent protein kinase (CaM kinase) II gamma	−3.40	**5** (7, 8, 19, 20, 28)	10q22

The numbers inside the parentheses correspond to the specific pathways in Table 2. Genes highlighted in red are also shown in Table 1.
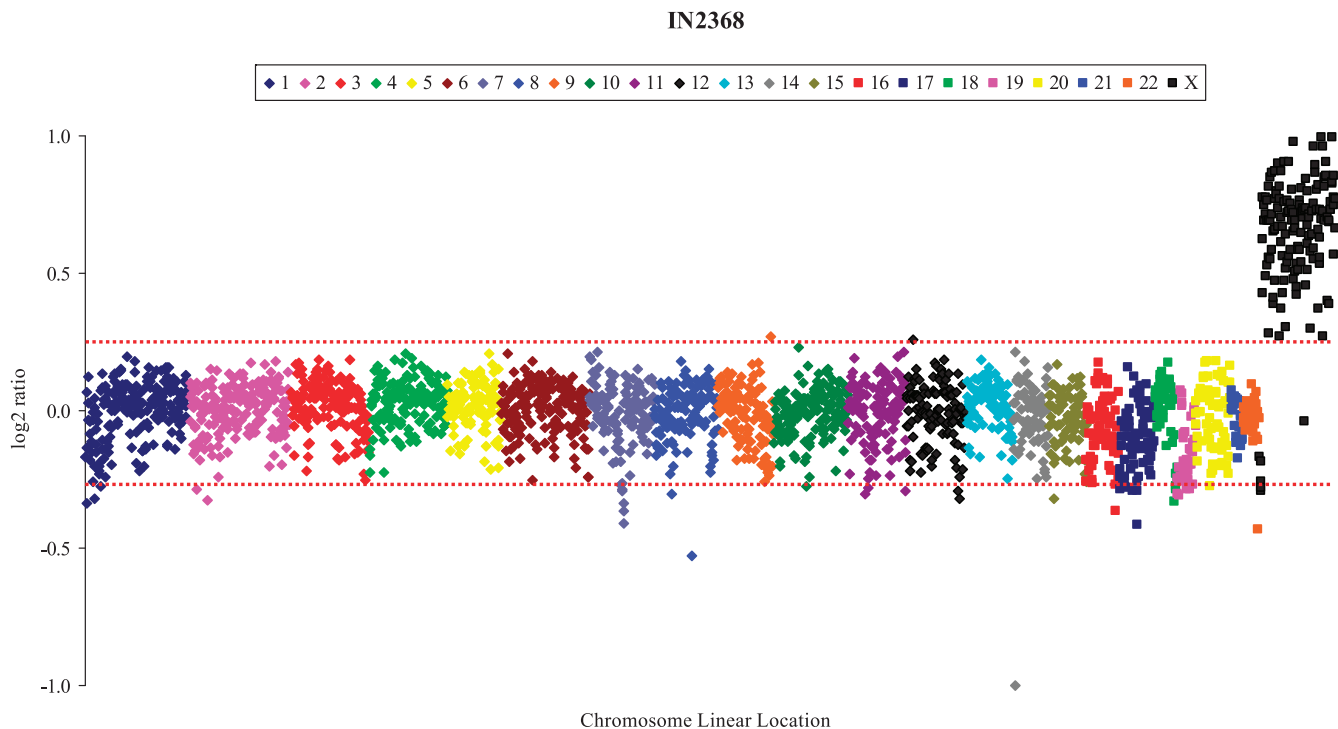
Figure 2. Combined dye swap aCGH profile for the tumor with the most aberrations, IN2368. Iterative linear regression global normalizations were used to reduce the SD of spot $\log_2$ ratios with an outlier range of $\pm 2SD$. Clones that showed a $\log_2$ ratio in excess of $\pm 3SD$ were deemed to be gained or lost (indicated by the red dotted line).

the normal samples (see Figure W2, *a* and *b*, for gel electrophoresis and sequencing results).

Discussion

This investigation has focused on the correlation between genomic CNAs at a 1-Mb resolution and global differential gene expression in PA. Overall, these data remain descriptive with the aims of identifying novel candidate target genes and characterizing cellular pathways that are involved in tumor development and growth. Future functional studies are needed to evaluate these targets in pediatric PA, but as discussed, evidence supports a role for these candidates in tumorigenesis.

Subgroups and Molecular Signatures in Pediatric PA

Unsupervised hierarchical clustering of PA in this study grouped tumor and control samples separately but further subgroups within PA were not identified. Wong et al. [16] previously demonstrated that two subgroups of PA could be distinguished by a molecular signature and suggested that these subgroups represented PA with different potentials of progression. Although it has been documented that pediatric PA that undergo partial excision may reoccur in the same location, malignant progression is rare [3,48]. In the PA included in our study, 13 of 89 genes from the molecular signature for which there were reliable data showed a continuous change in expression rather than a significant differential expression between two PA subgroups. However, the authors recognize that only a proportion of the genes could be investigated here in a smaller sample group compared to that of Wong et al. [16]. Sharma et al. [17] also reported a molecular signature of 36 genes with differential expression between supratentorial PA and posterior fossa PA and suggested that glial tumors have an intrinsic, lineage-specific signature that reflects the region of

the brain from which the nonmalignant tumor cell precursors originated. In the present tumor group, most tumors were located in the posterior fossa and, consequently, a comparison was not possible.

The characterization of molecular signatures that can distinguish PA arising in different locations or tumor subgroups emphasizes the intrinsic genetic heterogeneity of PA and the need for large sample numbers to identify valid subgroups with clinical or prognostic relevance.

Control Samples in Pediatric PA Microarray Analysis

The use of various controls to identify differentially expressed genes between normal and diseased samples in microarray experiments can directly influence those genes deemed to show differential gene expression, as reported by Zorn et al. [49] who investigated the choice of normal controls in the study of ovarian carcinoma. The normal controls used in previous microarray studies of brain tumors vary greatly. Studies comparing tumor expression profiles to normal brain have used total RNA from tissue samples obtained from normal brain regions including tissue from a lobectomy after edema, hippocampus tissue from a patient with epilepsy, subcortical white matter, cortical brain, the cortex of temporal lobe, and postmortem cortex, and medulla tissues [50–54]. Groups who have not had direct access to normal brain have also commercially purchased total RNA samples of adult and fetal normal brain for use as controls, including Wong et al. [16,50].

The control samples of this study are pooled adult normal whole-brain samples from a commercial source. This removes the chance of tumor contamination within the normal sample and using pooled normal samples reduces expression variations present in each individual. The decision to use adult normal total brain as a control was reached after detailed investigations of both fetal and adult brain from specific brain regions and whole brain (Figure W3).
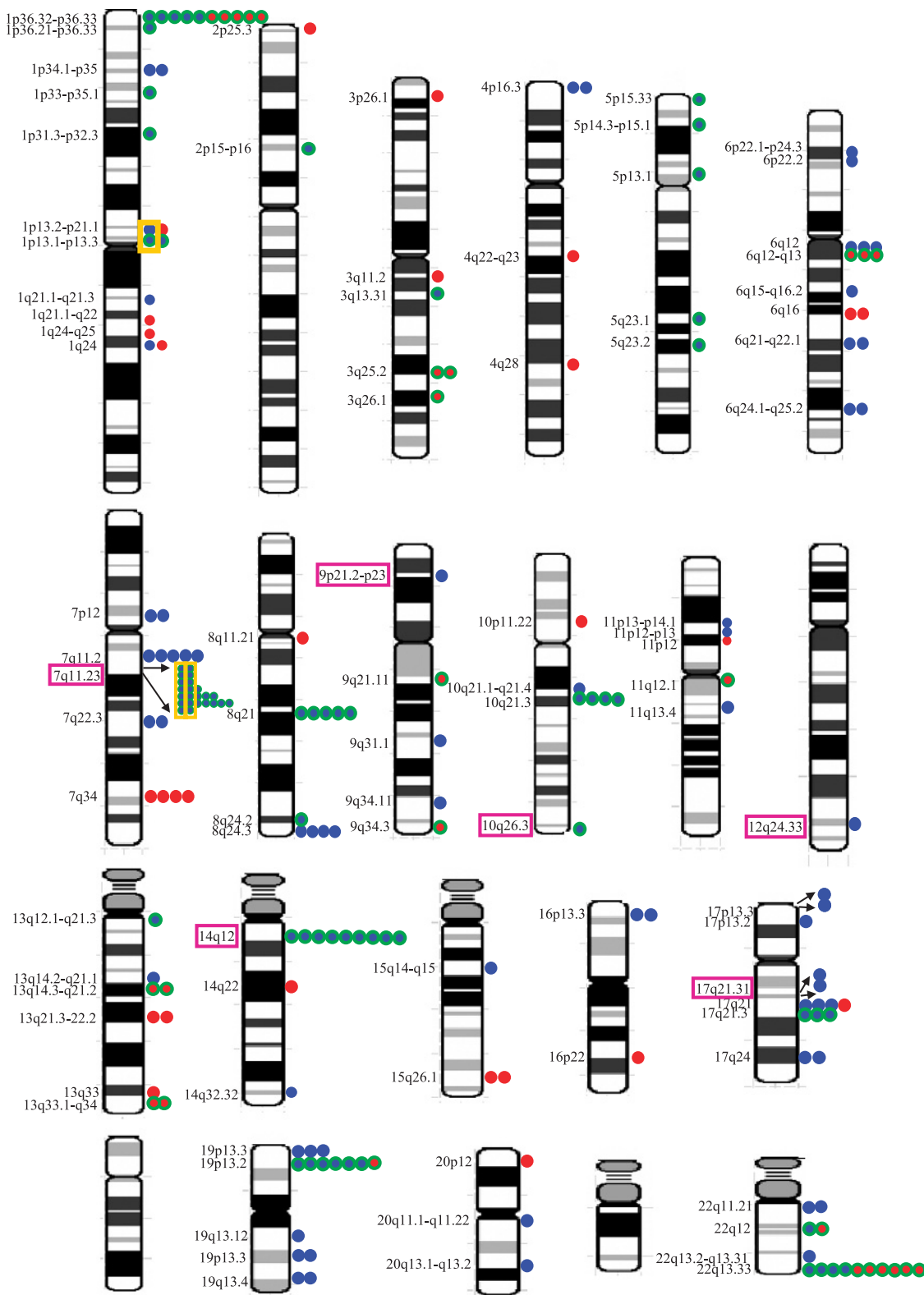
Figure 3. Results of aCGH analysis illustrating regions of chromosome gain and loss in pediatric PA. Circles to the right of each chromosome ideogram show the number of individual tumors with copy gains (red) and losses (blue) for each clone among the 11 PA studied. Clones in a region of copy number variation in the normal population are indicated by a green ring. Adjacent clones lost in the same tumor are indicated by a yellow box. Multiple clones in a region are indicated by two arrows. Correlations between clone CNAs and differential gene expression in the same region are indicated by a purple box.

Table 4. SD and SEM Are Derived from the Control Values from Normal DNA Obtained from Blood from Four Individuals and One Male and One Female Commercially Available Pooled DNA Samples (see Table W8 for Raw Data).

	Equation of Standard Curve	SD Normalized	SEM Normalized	95% Reference Range	Deletion ≤ Average Control Copy Number Minus 95% Reference Range	Gain ≥ Average Control Copy Number Plus 95% Reference Range
β-actin	$y = -3.4929x + 30.726$ $R^2 = 0.9928$					
1p36.32	$y = -3.3914x + 29.223$ $R^2 = 0.998$	0.05	0.02	0.09	0.91	1.09
BLC7B	$y = -3.4301x + 28.386$ $R^2 = 0.9814$	0.06	0.03	0.12	0.88	1.12
BLC7A	$y = -3.1059x + 28.599$ $R^2 = 0.9934$	0.05	0.02	0.10	0.90	1.10
14q12	$y = -3.2777x + 28.844$ $R^2 = 0.9979$	0.12	0.05	0.23	0.77	1.23
FOXG1B	$y = -3.0543x + 30.212$ $R^2 = 0.9935$	0.12	0.05	0.24	0.76	1.24

Hierarchical clustering of adult and fetal normal controls independently of the tumors suggested that either fetal or adult normal controls were suitable for the study of tumor biopsy samples. Furthermore, 1345 common differentially expressed probe sets were identified in the PA when using either adult or fetal normal controls. However, it was noted that fetal brain is in an exponential or linear growth phase and that this may affect gene expression and signaling pathways, masking aspects of the tumor profile if used as a control [55]. Increased proliferation, cell signaling, and reduced apoptosis are associated with fetal development and are characteristics of tumor cells. Furthermore, on investigation of the cellular pathways influenced by differential gene expression in the PA when adult or fetal normal controls were used and in the normal fetal controls when compared to adult normal controls, it became apparent that genes of the Wnt signaling pathway, cell cycle, and, to a lesser extent, the colorectal cancer pathway were up-regulated in the fetal normal controls compared to the adult normal controls and masked some differential gene expression in the PA. Moreover, the Wnt signaling pathway has been implicated in fetal development [56–60].

Variation was also seen between the expression profiles of total brain, cerebellum and corpus callosum from both adult and fetal origin. Furthermore, the tumors of this study are located in brain regions other than the cerebellum and corpus callosum, and it was felt inappropriate to compare tumors from different locations to normal controls taken from these regions, particularly because unique molecular signatures have been characterized from PA located in supratentorial and posterior fossa regions as previously discussed [17]. Consequently, to standardize the normal control group and reduce sample heterogeneity, four pooled adult whole-brain samples from between three and five individuals were selected as controls. Although variation can be seen between the four control samples, it is critical to note that if any one of these four is removed and the analysis repeated, the overall expression analysis results are unchanged with only minor differences in exact fold change values.

Genes Involved in Pediatric PA Development

To investigate pediatric PA development, those genes that showed a greater than 10-fold change in expression and were either involved in a KEGG pathway or were well characterized were identified. The overexpression of SERPINA3 and CHI3L1 provides evidence that the tumor cells are of astrocytic lineage. SERPINA3 is specifically expressed in astrocytes and is involved in the expression of astrocytic

Table 5. Relative Copy Number for Each Gene or Region Was Calculated as Follows: Deletion: ≤ Copy Number of Controls Minus 95% Reference Range of Controls (or 2SD of Controls), Gain: ≥ Copy Number of Controls Plus 95% Reference Range of Controls (or 2SD of Controls).

Tumor	1p36.32 (RP4-703E10) BAC array/RT-QPCR	BCL7B* BAC array/RT-QPCR	BCL7A (RP11-87C12) BAC array/RT-QPCR	14q12 (RP11-125A5) BAC array/RT-QPCR	FOXG1B Promoter[†] RT-QPCR
IN1740	Loss/0.54	No CNA/0.38	No CNA/0.53	No CNA/0.71	0.50
IN2356	ND/0.85	ND/0.88	ND/0.79	ND/0.62	1.07
IN2368	No CNA/1.05	Loss/0.31	No CNA/0.85	Loss/0.89	1.12
IN2524	Gain/1.22	Loss/1.08	No CNA/1.01	Loss/0.33	1.30
IN2631	Gain/1.17	No CNA/0.24	No CNA/1.10	Loss/1.10	0.95
IN2674	Loss/0.85	Loss/0.48	No CNA/0.51	Loss/0.85	1.04
IN2788	Loss/0.37	Loss/0.23	No CNA/0.29	No CNA/0.74	0.32
IN2825	ND/0.99	ND/0.66	ND/0.67	ND/0.96	0.69
IN2921	ND/0.93	ND1.03	ND/0.34	ND/0.90	0.38
IN2940	Loss/1.10	No CNA/0.59	No CNA/0.44	Loss/1.01	0.49
IN2969	Gain/0.61	No CNA/0.52	No CNA/0.48	Loss/0.91	0.55
IN3013	Loss/0.46	Loss/0.44	No CNA/0.35	Loss/0.47	0.32
IN3115	Gain/1.12	Loss/0.33	Loss/0.38	Loss/0.98	1.06
IN3156	ND/0.33	ND/0.35	ND/0.34	ND/0.28	0.48

BAC clone alterations for each region are indicated by loss or gain. Blue values correspond to deletions detected by RT-QPCR. Red values correspond to gains detected by RT-QPCR.
*BCL7B is not located under a specific clone but maps within the small region of loss encompassing up to seven clones at 7q11.23. ND indicates not done.
[†]FOXG1B maps adjacent to clone RP11-125A5 at 14q12.
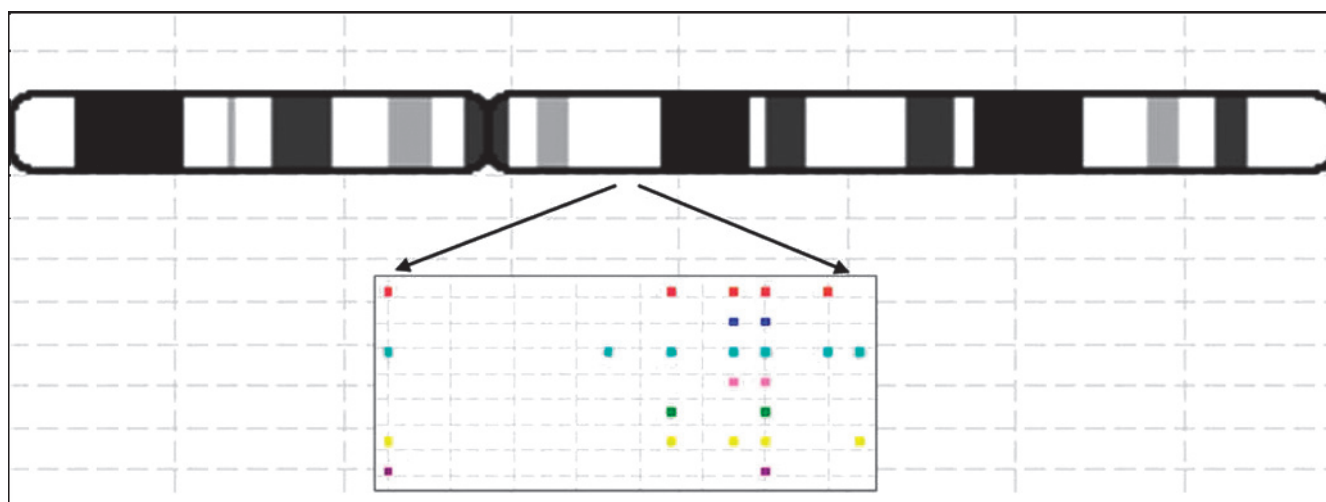
Figure 4. Loss of between two and seven contiguous BAC clones at 7q11.23 in seven PA. The rows of colored spots represent individual tumors and single BAC clones losses at 7q11.23. The distance between each spot is representative of the BAC clone binding locations on DNA.

markers such as glial fibrillary acidic protein (GFAP) [61,62]. *GFAP* was found to be 1.98-fold up-regulated in this study. *CHI3L1* is another astrocytic marker that has been used previously as a diagnostic indicator in astrocytoma [63,64].

Several genes listed in Table 1 have been investigated in other grades of astrocytoma including *T1A-2*, *ABCC3*, *CD44*, *MYT1*, *TIMP1*, *HLA-DPA1*, *TFPI*, *CSPG2*, *CD151*, *WNT10B*, *PTK2B*, *ENPP2*, *MBP*, *MATK*, *SST*, *CCK*, and *FOXG1B*. *T1A-2* expression was found to be significantly higher in glioblastoma multiforme (GBM) compared to anaplastic astrocytoma or diffuse astrocytoma, and it is a marker of malignant progression [65]. The large fold change in PA compared to normal brain suggests that this gene is involved in promoting PA development.

Other genes from this group have functions associated with a range of tumor characteristics. For example, increased expression of *ABCC3* from the multidrug-resistant protein family of ATP-dependent efflux pumps may mediate drug resistance in PA [66]. There is evidence to suggest that *CSPG2* protects from oxidative stress induced apoptosis and promotes tumor growth and angiogenesis [67]. Interestingly, *CPGS4* from the same family was found to be up-regulated in diffuse and malignant astrocytoma in response to platelet-derived growth factor (PDGF) and increases tumor cell proliferation and invasion [68,69]. In the present study, *CSPG2* and *CPGS4* demonstrated a 10.86- and 23.77-fold up-regulation in expression, respectively, in addition to *PDGFRA* that was also overexpressed by 5.84-fold.

The remaining genes listed in Table 1 either have been associated with the development of other tumors and cancers or have functions that could promote or inhibit tumor development. *POSTN*, for example, is overexpressed in more than 80% of human colon cancers and demonstrates the highest fold change expression in oral squamous cell carcinoma. *POSTN* enhances cancer growth by preventing stress-induced apoptosis and enhancing endothelial cell survival promoting angiogenesis [70,71].

Pathways with Differential Gene Expression in Pediatric PA

The Onto-Tools software ranked the KEGG pathways influenced by the 1844 differentially expressed genes according to the extent of disruption. In PA, the KEGG pathway antigen processing and presentation was most affected by differential gene expression. With the exception of *HSP90A*, all identified genes involved in this pathway were up-regulated, including *CD74*, *HLA-DPA1*, *HLA-DRA*, *HLA-DMA*, *HLA-DRB1*, *HLA-DMB*, *HLA-DQB1*, *HLA-G*, *CTSS*, *HLA-B*, *KLRC3*, *HLA-F*, *HLA-A*, *PSME2*, *PDIA3*, *HLA-E*, *IFI30*, *TAP1*, and *B2M*. A previous study noted an increase in the expression of genes involved in immune response in PA compared to diffuse astrocytoma, oligodendrogliomas, and normal brain [72]. An increase in *HLA-DPA1* expression in PA compared to anaplastic astrocytoma was also observed in a second study [73]. Furthermore, HLA-DR overexpression has been associated with good prognosis in large-bowel carcinoma and serous ovarian tumors [74,75]. The

Table 6. BAC Clone Losses and Differential Gene Expression in the Same Region in Pediatric PA.

Clone Location	Clone Name	Clone Alteration	Gene Located in Clone Region	Fold Change in Expression	Description
7q11.23	RP11-35P20, B315H11, CITB-51J22, B270D13, B39H04, RP11-137E8, RP11-89A20	Loss	*BCL7B*	−2.14	B-cell CLL/lymphoma 7B
9p21.2–p23	RP11-163F8	Loss	*SH3GL2*	−6.94	SH3-domain GRB2-like 2
10q26.3	RP11-122K13	Loss	*DRD1IP*	−35.09	Dopamine receptor D_1 interacting protein
12q24.33	RP11-87C12	Loss	*BCL7A*	−2.98	B-cell CLL/lymphoma 7A
14q12	RP11-125A5	Loss	*FOXG1B*	−325.73	Forkhead box G1B
17q21.31	AC100793.8	Loss	*TUBG2*	−2.28	Tubulin, gamma 2
			CNTNAP1	−2.99	Contactin-associated protein 1

up-regulation of immune response genes in PA may contribute to the benign behavior of this tumor type.

The KEGG phosphatidylinositol (PI3K) signaling system and the mitogen-activated protein kinase (MAPK) signaling pathway are ranked as the third and fifth, respectively, according to the extent of differential gene expression in PA (Table 2). Altered signaling in these pathways through increased receptor stimulation and disrupted tumor suppressor or oncogene function has been characterized in other grades of astrocytoma particularly primary and secondary adult GBM [76].

Genomic Aberrations Previously Identified in Pediatric PA

Few studies have identified nonrandom whole-chromosome or arm aberrations in PA of the pediatric population. As discussed in the introduction, Jones et al. [25] only identified CNAs in children older than 10 years using aCGH. Furthermore, using analog CGH, Sanoudou et al. [5] identified five PA (12%) with whole-chromosome aberrations, and all were from patients 7 years or older (four patients were 10 years or older). Of the tumors in this study, 59% were from patients older than 7 years and 41% were from patients older than 10 years. Possibly, whole-chromosome or arm aberrations maybe more common in PA of older children. In our study, five cases (45%) were from patients 7 years or older and only one case was from a patient older than 10 years. This may explain why we have not identified any whole-chromosome or arm aberrations in the tumors of this patient cohort.

Genomic Loss in Regions of LCVs in Pediatric PA

Of 97 BAC clones altered in PA, 40% were located in regions of LCV present in the normal population [77–84]. The role of LCVs (which involve gain or loss of hundreds of kilobases of genomic DNA) in phenotypically normal individuals is not clear [77]. However, LCVs at 14q12 were found to be present in DNA from 50% of chronic myeloid leukemia and pediatric solid tumors compared to an incidence of 10% in somatic DNA of healthy control individuals, suggesting that acquired or inherited LCVs at 14q12 may be associated with the onset or progression of neoplasia [85]. In our study, the incidence of 14q12 aberrations in PA was 79%, as identified by combined aCGH and RT-QPCR analyses. Further investigations are necessary to establish the incidence of LCVs in somatic DNA of PA patients to determine whether 14q12 aberrations are inherited or are acquired during tumor development.

Correlation of CNAs and Gene Expression in Pediatric PA

Loss of individual clones at 9p21.2–p23, 10q26.3, 12q24.33, and 17q21.31 and a small region of up to seven adjacent clones at 7q11.23 correlated with differential gene expression. Crucially, although BAC array analysis did not identify genomic loss in all tumors, the down-regulation of genes including SH3GL2 at 9p21.2–p23, DRD1IP at 10q26.3, BCL7A at 12q24.33, TUB2 and CNTNAP1 at 17q21.31, and BCL7B at 7q11.23 was seen in all cases. Furthermore, RT-QPCR analysis of relative DNA copy number of BCL7B at 7q11.23 and BCL7A at 12q24.33 identified loss in 12 (86%) of 14 tumors. BCL7B and BCL7A are from the same gene family and share 90% homology. BCL7B maps to a region deleted in the congenital disorder Williams syndrome, although little is known about its function [86]. BCL7A is a putative tumor suppressor gene, which is hypermethylated in the primary cutaneous T-cell lymphoma [87]. Earlier studies have demonstrated the involvement of the BCL7A locus in a recurrent

break point in B-cell lymphomas and a complex translocation and rearrangement in specific cell lines [88]. Expression profiling of mycosis fungoides, a common cutaneous T-cell lymphoma and B-cell lymphoma, identified the down-regulation of BCL7A as part of molecular signatures that could distinguish mycosis fungoides and inflammatory dermatoses and distinct types of diffuse large B-cell lymphoma [89,90]. The loss of BCL7A has also been associated with disrupted NF-κB signaling and unfavorable prognosis in patients with B-cell lymphomas, suggesting that this gene has tumor suppressor properties [91].

The clone aberrations detected at 14q12 by BAC array analysis could only be confirmed by RT-QPCR in two cases. A previous study also failed to confirm RP11-125A5 loss [47]. This region is a common site for duplication and deletion events in hepatoblastoma, which may explain the discrepancies between CNA detected by BAC array and RT-QPCR analysis in the PA of this study [92]. However, FOXG1B maps adjacent to clone RP11-125A5 and shows significant down-regulation in all PA. Real-time quantitative polymerase chain reaction analysis of relative DNA copy number of the FOXG1B promoter demonstrated genomic loss in almost 60% of tumors examined, indicating that genomic loss is an important mechanism in the underexpression of this gene.

FOXG1B is an oncogenic transformer and transcriptional repressor, which interacts with Groucho, Hes, and Smad proteins [93,94]. More importantly, FOXG1B has been proposed as a major FoxO forkhead transcription factor that acts as a signal transducer between the Smad, PI3K, and FoxG1B pathways. The activity of these pathway interactions has been shown to be involved in the resistance to transforming growth factor beta (TGFβ)–mediated cytostasis during telencephalic neuroepithelium development and in GBM cells [95]. The involvement of FOXG1B in PI3K (the pathway most affected by the differential gene expression in PA) highlights the impact FOXG1B disruption may have on intracellular signaling. The location of this gene in a region of LCV at 14q12 also suggests that some individuals may be predisposed to PA development.

Reduction of SH3GL2 expression correlated with loss at 9p21.2–p23. A recent study indicates that SH3GL2 is involved in the development and progression of laryngeal squamous cell carcinoma and expression levels correlate with pathologic classification [96]. The expression of SH3GL2 also correlates with distinct stages of intestinal-type gastric cancer, although a functional role in tumorigenesis has not yet been determined [97].

TUBG2, located at 17q21.31, shares 97.3% amino acid identity with TUBG1, and the two genes are coexpressed in a variety of tissues. This suggests that the functions of TUBG1 and TUBG2 are similar, both having a significant role in the organization of the microtubule cytoskeleton [98]. CNTNAP1, also located at 17q21.31, is transcribed predominantly in the brain, and the architecture of the protein extracellular domain is similar to that of neurexins. CNTNAP1 plays an important role in the creation and maintenance of paranodal regions of myelinated axons, enabling recruitment and activation of intracellular signaling pathways in neurons [99]. DRD1IP maps to 10q26.3 and encodes a brain-specific dopamine receptor 1–interacting protein involved in calcium signaling [100]. A role for these genes in tumor development has yet to be established.

Promoter Hypermethylation in Pediatric PA

Down-regulation of gene expression through promoter hypermethylation is an important mechanism of transcriptional silencing in many tumors. Hypermethylation of the six genes investigated in

this study has been detected in more than 30% of gastric carcinoma, lung cancer, and renal cell carcinoma. Moreover, *CCNA1* was hypermethylated in 100% of colorectal adenoma [28–33]. All six genes demonstrated a twofold and significant down-regulation in PA compared to normal brain, but hypermethylation of gene promoter regions was not detected. Only one previous study has investigated hypermethylation in pediatric PA involving *MGMT, GSTP1, DAPK1, $p14^{ARF}$, THBS-1, TIMP-3, p73, $p16^{INK4A}$*, *RB-1*, and *TP53*. Hypermethylation of $p16^{INK4A}$ was most frequent occurring in 46% of cases. However, five of the remaining genes were hypermethylated in less than 8% of cases [101]. It is possible that methylation is not the predominant mechanism of gene silencing in PA development but that other epigenetic processes such as histone modification and microRNA play a more significant role.

We have clearly demonstrated that PA have distinct expression profiles compared to normal whole brain. We have identified two key signaling pathways (PI3K and MAPK) that contribute toward tumor development. Large regions of chromosome alterations were not identified in PA, although 97 individual BAC clones and a small region on chromosome 7 were lost and/or gained. This is the first study to establish a correlation between small regions of genomic CNA and differential gene expression in PA. The down-regulation of gene family members *BCL7B* and *BCL7A* due to independent CNAs suggests a tumor suppressor role for these genes in PA. Furthermore, we have demonstrated that genomic alterations in a region of LCV at 14q12 may predispose individuals to tumor development. The accompanying loss of *FOXG1B* expression in all samples together with its involvement in PI3K signaling provides compelling evidence that this gene may play a significant role in the development of pediatric PA.

Acknowledgments

References

[1] Kleihues P and Cavenee WK (2000). *Pathology and Genetics of Tumours of the Central Nervous System.* Lyon, France: IARC Press.

[2] Gajjar A, Sanford RA, Heideman R, Jenkins JJ, Walter A, Li Y, Langston JW, Muhlbauer M, Boyett JM, and Kun LE (1997). Low-grade astrocytoma: a decade of experience at St. Jude Children's Research Hospital. *J Clin Oncol* **8**, 2792–2799.

[3] Fernandez C, Figarella-Branger D, Girard N, Bouvier-Labit C, Gouvernet J, Paz PA, and Lena G (2003). Pilocytic astrocytomas in children: prognostic factors—a retrospective study of 80 cases. *Neurosurgery* **3**, 544–553.

[4] Rickert CH and Paulus W (2004). Comparative genomic hybridization in central and peripheral nervous system tumors of childhood and adolescence. *J Neuropathol Exp Neurol* **5**, 399–417.

[5] Sanoudou D, Tingby O, Ferguson-Smith MA, Collins VP, and Coleman N (2000). Analysis of pilocytic astrocytoma by comparative genomic hybridization. *Br J Cancer* **6**, 1218–1222.

[6] Shlomit R, Ayala AG, Michal D, Ninett A, Frida S, Boleslaw G, Gad B, Gideon R, and Shlomi C (2000). Gains and losses of DNA sequences in childhood brain tumors analyzed by comparative genomic hybridization. *Cancer Genet Cytogenet* **1**, 67–72.

[7] White FV, Anthony DC, Yunis EJ, Tarbell NJ, Scott RM, and Schofield DE (1995). Nonrandom chromosomal gains in pilocytic astrocytomas of childhood. *Hum Pathol* **9**, 979–986.

[8] Zattara-Cannoni H, Gambarelli D, Lena G, Dufour H, Choux M, Grisoli F, and Vagner-Capodano AM (1998). Are juvenile pilocytic astrocytomas benign tumors? A cytogenetic study in 24 cases. *Cancer Genet Cytogenet* **2**, 157–160.

[9] Phelan CM, Liu L, Ruttledge MH, Muntzning K, Ridderheim PA, and Collins VP (1995). Chromosome 17 abnormalities and lack of *TP53* mutations in paediatric central nervous system tumours. *Hum Genet* **6**, 684–690.

[10] von Deimling A, Louis DN, Menon AG, von Ammon K, Petersen I, Ellison D, Wiestler OD, and Seizinger BR (1993). Deletions on the long arm of chromosome 17 in pilocytic astrocytoma. *Acta Neuropathol (Berl)* **1**, 81–85.

[11] Willert JR, Daneshvar L, Sheffield VC, and Cogen PH (1995). Deletion of chromosome arm 17p DNA sequences in pediatric high-grade and juvenile pilocytic astrocytomas. *Genes Chromosomes Cancer* **3**, 165–172.

[12] Hayes VM, Dirven CM, Dam A, Verlind E, Molenaar WM, Mooij JJ, Hofstra RM, and Buys CH (1999). High frequency of *TP53* mutations in juvenile pilocytic astrocytomas indicates role of *TP53* in the development of these tumors. *Brain Pathol* **3**, 463–467.

[13] Patt S, Gries H, Giraldo M, Cervos-Navarro J, Martin H, Janisch W, and Brockmoller J (1996). *p53* gene mutations in human astrocytic brain tumors including pilocytic astrocytomas. *Hum Pathol* **6**, 586–589.

[14] Bertucci F, Finetti P, Rougemont J, Charafe-Jauffret E, Cervera N, Tarpin C, Nguyen C, Xerri L, Houlgatte R, Jacquemier J, et al. (2005). Gene expression profiling identifies molecular subtypes of inflammatory breast cancer. *Cancer Res* **6**, 2170–2178.

[15] Tay ST, Leong SH, Yu K, Aggarwal A, Tan SY, Lee CH, Wong K, Visvanathan J, Lim D, Wong WK, et al. (2003). A combined comparative genomic hybridization and expression microarray analysis of gastric cancer reveals novel molecular subtypes. *Cancer Res* **12**, 3309–3316.

[16] Wong KK, Chang YM, Tsang YT, Perlaky L, Su J, Adesina A, Armstrong DL, Bhattacharjee M, Dauser R, Blaney SM, et al. (2005). Expression analysis of juvenile pilocytic astrocytomas by oligonucleotide microarray reveals two potential subgroups. *Cancer Res* **1**, 76–84.

[17] Sharma MK, Mansur DB, Reifenberger G, Perry A, Leonard JR, Aldape KD, Albin MG, Emnett RJ, Loeser S, Watson MA, et al. (2007). Distinct genetic signatures among pilocytic astrocytomas relate to their brain region origin. *Cancer Res* **3**, 890–900.

[18] Cai WW, Mao JH, Chow CW, Damani S, Balmain A, and Bradley A (2002). Genome-wide detection of chromosomal imbalances in tumors using BAC microarrays. *Nat Biotechnol* **4**, 393–396.

[19] Misra A, Pellarin M, Nigro J, Smirnov I, Moore D, Lamborn KR, Pinkel D, Albertson DG, and Feuerstein BG (2005). Array comparative genomic hybridization identifies genetic subgroups in grade 4 human astrocytoma. *Clin Cancer Res* **8**, 2907–2918.

[20] Nigro JM, Misra A, Zhang L, Smirnov I, Colman H, Griffin C, Ozburn N, Chen M, Pan E, Koul D, et al. (2005). Integrated array-comparative genomic hybridization and expression array profiles identify clinically relevant molecular subtypes of glioblastoma. *Cancer Res* **5**, 1678–1686.

[21] Rossi MR, La DJ, Matsui S, Nowak NJ, Hawthorn L, and Cowell JK (2005). Novel amplicons on the short arm of chromosome 7 identified using high resolution array CGH contain over expressed genes in addition to EGFR in glioblastoma multiforme. *Genes Chromosomes Cancer* **4**, 392–404.

[22] Ruano Y, Mollejo M, Ribalta T, Fiano C, Camacho FI, Gomez E, de Lope AR, Hernandez-Moneo JL, Martinez P, and Melendez B (2006). Identification of novel candidate target genes in amplicons of glioblastoma multiforme tumors detected by expression and CGH microarray profiling. *Mol Cancer* **5**, 39.

[23] Vranova V, Necesalova E, Kuglik P, Cejpek P, Pesakova M, Budinska E, Relichova J, and Veselska R (2007). Screening of genomic imbalances in glioblastoma multiforme using high-resolution comparative genomic hybridization. *Oncol Rep* **2**, 457–464.

[24] Wrensch M, McMillan A, Wiencke J, Wiemels J, Kelsey K, Patoka J, Jones H, Carlton V, Miike R, Sison J, et al. (2007). Nonsynonymous coding single-nucleotide polymorphisms spanning the genome in relation to glioblastoma survival and age at diagnosis. *Clin Cancer Res* **1**, 197–205.

[25] Jones DT, Ichimura K, Liu L, Pearson DM, Plant K, and Collins VP (2006). Genomic analysis of pilocytic astrocytomas at 0.97 Mb resolution shows an increasing tendency toward chromosomal copy number change with age. *J Neuropathol Exp Neurol* **11**, 1049–1058.

[26] Wong KK, Tsang YT, Chang YM, Su J, Di Francesco AM, Meco D, Riccardi R, Perlaky L, Dauser RC, Adesina A, et al. (2006). Genome-wide allelic imbalance analysis of pediatric gliomas by single nucleotide polymorphic allele array. *Cancer Res* **23**, 11172–11178.

[27] Costello JF, Plass C, and Cavenee WK (2000). Aberrant methylation of genes in low-grade astrocytomas. *Brain Tumor Pathol* **2**, 49–56.

[28] Kikuchi T, Toyota M, Itoh F, Suzuki H, Obata T, Yamamoto H, Kakiuchi H, Kusano M, Issa JP, Tokino T, et al. (2002). Inactivation of $p57^{KIP2}$ by regional promoter hypermethylation and histone deacetylation in human tumors. *Oncogene* **17**, 2741–2749.

[29] Morris MR, Gentle D, Abdulrahman M, Maina EN, Gupta K, Banks RE, Wiesener MS, Kishida T, Yao M, Teh B, et al. (2005). Tumor suppressor activity and epigenetic inactivation of hepatocyte growth factor activator inhibitor type 2/SPINT2 in papillary and clear cell renal cell carcinoma. *Cancer Res* **11**, 4598–4606.

[30] Oshimo Y, Oue N, Mitani Y, Nakayama H, Kitadai Y, Yoshida K, Chayama K, and Yasui W (2004). Frequent epigenetic inactivation of RIZ1 by promoter hypermethylation in human gastric carcinoma. *Int J Cancer* **2**, 212–218.

[31] Takahashi T, Suzuki M, Shigematsu H, Shivapurkar N, Echebiri C, Nomura M, Stastny V, Augustus M, Wu CW, Wistuba II, et al. (2005). Aberrant methylation of *Reprimo* in human malignancies. *Int J Cancer* **4**, 503–510.

[32] Toyooka S, Toyooka KO, Miyajima K, Reddy JL, Toyota M, Sathyanarayana UG, Padar A, Tockman MS, Lam S, Shivapurkar N, et al. (2003). Epigenetic down-regulation of death-associated protein kinase in lung cancers. *Clin Cancer Res* **8**, 3034–3041.

[33] Xu XL, Yu J, Zhang HY, Sun MH, Gu J, Du X, Shi DR, Wang P, Yang ZH, and Zhu JD (2004). Methylation profile of the promoter CpG islands of 31 genes that may contribute to colorectal carcinogenesis. *World J Gastroenterol* **23**, 3441–3454.

[34] Sowar K, Straessle J, Donson AM, Handler M, and Foreman NK (2006). Predicting which children are at risk for ependymoma relapse. *J Neurooncol* **1**, 41–46.

[35] Draghici S, Khatri P, Bhavsar P, Shah A, Krawetz SA, and Tainsky MA (2003). Onto-Tools, the toolkit of the modern biologist: Onto-Express, Onto-Compare, Onto-Design and Onto-Translate. *Nucleic Acids Res* **13**, 3775–3781.

[36] Khatri P, Sellamuthu S, Malhotra P, Amin K, Done A, and Draghici S (2005). Recent additions and improvements to the Onto-Tools. *Nucleic Acids Res* **33** (Web Server issue), W762–W765.

[37] Kanehisa M and Goto S (2000). KEGG: Kyoto encyclopedia of genes and genomes. *Nucleic Acids Res* **1**, 27–30.

[38] Saeed AI, Sharov V, White J, Li J, Liang W, Bhagabati N, Braisted J, Klapa M, Currier T, Thiagarajan M, et al. (2003). TM4: a free, open-source system for microarray data management and analysis. *Biotechniques* **2**, 374–378.

[39] Yang YH, Dudoit S, Luu P, Lin DM, Peng V, Ngai J, and Speed TP (2002). Normalization for cDNA microarray data: a robust composite method addressing single and multiple slide systematic variation. *Nucleic Acids Res* **4**, e15.

[40] Quackenbush J (2002). Microarray data normalization and transformation. *Nat Genet* **32 Suppl**, 496–501.

[41] Finkelstein DB, Gollub J, Ewing R, Sterky F, Somerville S, and Cherry JM (2002). Iterative linear regression by sector: renormalization of cDNA microarray data and cluster analysis weighted by cross homology. In *Methods of Microarray Analysis*. SM Lin and KF Johnson (Eds.) (unpublished work).

[42] Senchenko V, Liu J, Braga E, Mazurenko N, Loginov W, Seryogin Y, Bazov I, Protopopov A, Kisseljov FL, Kashuba V, et al. (2003). Deletion mapping using quantitative real-time PCR identifies two distinct 3p21.3 regions affected in most cervical carcinomas. *Oncogene* **19**, 2984–2992.

[43] Suarez-Merino B, Hubank M, Revesz T, Harkness W, Hayward R, Thompson D, Darling JL, Thomas DG, and Warr TJ (2005). Microarray analysis of pediatric ependymoma identifies a cluster of 112 candidate genes including four transcripts at 22q12.1–q13.3. *Neuro Oncol* **1**, 20–31.

[44] Olek A, Oswald J, and Walter J (1996). A modified and improved method for bisulphite based cytosine methylation analysis. *Nucleic Acids Res* **24**, 5064–5066.

[45] Warnecke PM, Stirzaker C, Melki JR, Millar DS, Paul CL, and Clark SJ (1997). Detection and measurement of PCR bias in quantitative methylation analysis of bisulphite-treated DNA. *Nucleic Acids Res* **21**, 4422–4426.

[46] Coe BP, Ylstra B, Carvalho B, Meijer GA, Macaulay C, and Lam WL (2007). Resolving the resolution of array CGH. *Genomics* **5**, 647–653.

[47] Qiao Y, Liu X, Harvard C, Nolin SL, Brown WT, Koochek M, Holden JJ, Lewis ME, and Rajcan-Separovic E (2007). Large-scale copy number variants (CNVs): distribution in normal subjects and FISH/real-time qPCR analysis. *BMC Genomics* **8**, 167.

[48] Krieger MD, Gonzalez-Gomez I, Levy ML, and McComb JG (1997). Recurrence patterns and anaplastic change in a long-term study of pilocytic astrocytomas. *Pediatr Neurosurg* **1**, 1–11.

[49] Zorn KK, Jazaeri AA, Awtrey CS, Gardner GJ, Mok SC, Boyd J, and Birrer MJ (2003). Choice of normal ovarian control influences determination of differentially expressed genes in ovarian cancer expression profiling studies. *Clin Cancer Res* **13**, 4811–4818.

[50] Godard S, Getz G, Delorenzi M, Farmer P, Kobayashi H, Desbaillets I, Nozaki M, Diserens AC, Hamou MF, Dietrich PY, et al. (2003). Classification of human astrocytic gliomas on the basis of gene expression: a correlated group of genes with angiogenic activity emerges as a strong predictor of subtypes. *Cancer Res* **20**, 6613–6625.

[51] Huang H, Colella S, Kurrer M, Yonekawa Y, Kleihues P, and Ohgaki H (2000). Gene expression profiling of low-grade diffuse astrocytomas by cDNA arrays. *Cancer Res* **24**, 6868–6874.

[52] Khatua S, Peterson KM, Brown KM, Lawlor C, Santi MR, LaFleur B, Dressman D, Stephan DA, and MacDonald TJ (2003). Overexpression of the EGFR/FKBP12/HIF-2alpha pathway identified in childhood astrocytomas by angiogenesis gene profiling. *Cancer Res* **8**, 1865–1870.

[53] Rickman DS, Bobek MP, Misek DE, Kuick R, Blaivas M, Kurnit DM, Taylor J, and Hanash SM (2001). Distinctive molecular profiles of high-grade and low-grade gliomas based on oligonucleotide microarray analysis. *Cancer Res* **18**, 6885–6891.

[54] Shai R, Shi T, Kremen TJ, Horvath S, Liau LM, Cloughesy TF, Mischel PS, and Nelson SF (2003). Gene expression profiling identifies molecular subtypes of gliomas. *Oncogene* **31**, 4918–4923.

[55] Samuelsen GB, Larsen KB, Bogdanovic N, Laursen H, Graem N, Larsen JF, and Pakkenberg B (2003). The changing number of cells in the human fetal forebrain and its subdivisions: a stereological analysis. *Cereb Cortex* **2**, 115–122.

[56] Katoh M, Kirikoshi H, Saitoh T, Sagara N, and Koike J (2000). Alternative splicing of the *WNT-2B/WNT-13* gene. *Biochem Biophys Res Commun* **1**, 209–216.

[57] McMahon AP and Bradley A (1990). The *Wnt-1* (*int-1*) proto-oncogene is required for development of a large region of the mouse brain. *Cell* **6**, 1073–1085.

[58] Parr BA, Shea MJ, Vassileva G, and McMahon AP (1993). Mouse *Wnt* genes exhibit discrete domains of expression in the early embryonic CNS and limb buds. *Development* **1**, 247–261.

[59] Hoang BH, Thomas JT, bdul-Karim FW, Correia KM, Conlon RA, Luyten FP, and Ballock RT (1998). Expression pattern of two Frizzled-related genes, *Frzb-1* and *Sfrp-1*, during mouse embryogenesis suggests a role for modulating action of Wnt family members. *Dev Dyn* **3**, 364–372.

[60] Smalley MJ and Dale TC (1999). Wnt signalling in mammalian development and cancer. *Cancer Metastasis Rev* **2**, 215–230.

[61] Gopalan SM, Wilczynska KM, Konik BS, Bryan L, and Kordula T (2006). Nuclear factor-1-X regulates astrocyte-specific expression of the alpha1-antichymotrypsin and glial fibrillary acidic protein genes. *J Biol Chem* **19**, 13126–13133.

[62] Gopalan SM, Wilczynska KM, Konik BS, Bryan L, and Kordula T (2006). Astrocyte-specific expression of the alpha1-antichymotrypsin and glial fibrillary acidic protein genes requires activator protein-1. *J Biol Chem* **4**, 1956–1963.

[63] Rousseau A, Nutt CL, Betensky RA, Iafrate AJ, Han M, Ligon KL, Rowitch DH, and Louis DN (2006). Expression of oligodendroglial and astrocytic lineage markers in diffuse gliomas: use of YKL-40, ApoE, ASCL1, and NKX2-2. *J Neuropathol Exp Neurol* **12**, 1149–1156.

[64] Nutt CL, Betensky RA, Brower MA, Batchelor TT, Louis DN, and Stemmer-Rachamimov AO (2005). YKL-40 is a differential diagnostic marker for histologic subtypes of high-grade gliomas. *Clin Cancer Res* **6**, 2258–2264.

[65] Mishima K, Kato Y, Kaneko MK, Nishikawa R, Hirose T, and Matsutani M (2006). Increased expression of podoplanin in malignant astrocytic tumors as a novel molecular marker of malignant progression. *Acta Neuropathol (Berl)* **5**, 483–488.

[66] Bronger H, Konig J, Kopplow K, Steiner HH, Ahmadi R, Herold-Mende C, Keppler D, and Nies AT (2005). ABCC drug efflux pumps and organic anion uptake transporters in human gliomas and the blood–tumor barrier. *Cancer Res* **24**, 11419–11428.

[67] Zheng PS, Wen J, Ang LC, Sheng W, Viloria-Petit A, Wang Y, Wu Y, Kerbel RS, and Yang BB (2004). Versican/PG-M G3 domain promotes tumor growth and angiogenesis. *FASEB J* **6**, 754–756.

[68] Johansson FK, Goransson H, and Westermark B (2005). Expression analysis of genes involved in brain tumor progression driven by retroviral insertional mutagenesis in mice. *Oncogene* **24**, 3896–3905.

[69] Chekenya M, Rooprai HK, Davies D, Levine JM, Butt AM, and Pilkington GJ (1999). The NG2 chondroitin sulfate proteoglycan: role in malignant progression of human brain tumours. *Int J Dev Neurosci* **5–6**, 421–435.

[70] Bao S, Ouyang G, Bai X, Huang Z, Ma C, Liu M, Shao R, Anderson RM, Rich JN, and Wang XF (2004). Periostin potently promotes metastatic growth of colon cancer by augmenting cell survival via the Akt/PKB pathway. *Cancer Cell* **4**, 329–339.

[71] Siriwardena BS, Kudo Y, Ogawa I, Kitagawa M, Kitajima S, Hatano H, Tilakaratne WM, Miyauchi M, and Takata T (2006). Periostin is frequently overexpressed and enhances invasion and angiogenesis in oral cancer. *Br J Cancer* **10**, 1396–1403.

[72] Huang H, Hara A, Homma T, Yonekawa Y, and Ohgaki H (2005). Altered expression of immune defense genes in pilocytic astrocytomas. *J Neuropathol Exp Neurol* **10**, 891–901.

[73] Hunter S, Young A, Olson J, Brat DJ, Bowers G, Wilcox JN, Jaye D, Mendrinos S, and Neish A (2002). Differential expression between pilocytic and anaplastic astrocytomas: identification of apolipoprotein D as a marker for low-grade, non-infiltrating primary CNS neoplasms. *J Neuropathol Exp Neurol* **3**, 275–281.

[74] Lovig T, Andersen SN, Thorstensen L, Diep CB, Meling GI, Lothe RA, and Rognum TO (2002). Strong HLA-DR expression in microsatellite stable carcinomas of the large bowel is associated with good prognosis. *Br J Cancer* **7**, 756–762.

[75] Tamiolakis D, Kotini A, Venizelos J, Jivannakis T, Simopoulos C, and Papadopoulos N (2003). Prognostic significance of HLA-DR antigen in serous ovarian tumors. *Clin Exp Med* **2**, 113–118.

[76] Soni D, King JA, Kaye AH, and Hovens CM (2005). Genetics of glioblastoma multiforme: mitogenic signaling and cell cycle pathways converge. *J Clin Neurosci* **1**, 1–5.

[77] Iafrate AJ, Feuk L, Rivera MN, Listewnik ML, Donahoe PK, Qi Y, Scherer SW, and Lee C (2004). Detection of large-scale variation in the human genome. *Nat Genet* **9**, 949–951.

[78] Locke DP, Sharp AJ, McCarroll SA, McGrath SD, Newman TL, Cheng Z, Schwartz S, Albertson DG, Pinkel D, Altshuler DM, et al. (2006). Linkage disequilibrium and heritability of copy-number polymorphisms within duplicated regions of the human genome. *Am J Hum Genet* **2**, 275–290.

[79] Sebat J, Lakshmi B, Troge J, Alexander J, Young J, Lundin P, Maner S, Massa H, Walker M, Chi M, et al. (2004). Large-scale copy number polymorphism in the human genome. *Science* **5683**, 525–528.

[80] Fiegler H, Redon R, Andrews D, Scott C, Andrews R, Carder C, Clark R, Dovey O, Ellis P, Feuk L, et al. (2006). Accurate and reliable high-throughput detection of copy number variation in the human genome. *Genome Res* **12**, 1566–1574.

[81] Khaja R, Zhang J, MacDonald JR, He Y, Joseph-George AM, Wei J, Rafiq MA, Qian C, Shago M, Pantano L, et al. (2006). Genome assembly comparison identifies structural variants in the human genome. *Nat Genet* **12**, 1413–1418.

[82] Redon R, Ishikawa S, Fitch KR, Feuk L, Perry GH, Andrews TD, Fiegler H, Shapero MH, Carson AR, Chen W, et al. (2006). Global variation in copy number in the human genome. *Nature* **7118**, 444–454.

[83] Conrad DF, Andrews TD, Carter NP, Hurles ME, and Pritchard JK (2006). A high-resolution survey of deletion polymorphism in the human genome. *Nat Genet* **1**, 75–81.

[84] Sharp AJ, Locke DP, McGrath SD, Cheng Z, Bailey JA, Vallente RU, Pertz LM, Clark RA, Schwartz S, Segraves R, et al. (2005). Segmental duplications and copy-number variation in the human genome. *Am J Hum Genet* **1**, 78–88.

[85] Braude I, Vukovic B, Prasad M, Marrano P, Turley S, Barber D, Zielenska M, and Squire JA (2006). Large scale copy number variation (CNV) at 14q12 is associated with the presence of genomic abnormalities in neoplasia. *BMC Genomics* **7**, 138.

[86] Jadayel DM, Osborne LR, Coignet LJ, Zani VJ, Tsui LC, Scherer SW, and Dyer MJ (1998). The BCL7 gene family: deletion of *BCL7B* in Williams syndrome. *Gene* **1–2**, 35–44.

[87] van Doorn R, Zoutman WH, Dijkman R, de Menezes RX, Commandeur S, Mulder AA, van der Velden PA, Vermeer MH, Willemze R, Yan PS, et al. (2005). Epigenetic profiling of cutaneous T-cell lymphoma: promoter hypermethylation of multiple tumor suppressor genes including *BCL7a*, *PTPRG*, and *p73*. *J Clin Oncol* **17**, 3886–3896.

[88] Zani VJ, Asou N, Jadayel D, Heward JM, Shipley J, Nacheva E, Takasuki K, Catovsky D, and Dyer MJ (1996). Molecular cloning of complex chromosomal translocation t(8;14;12)(q24.1;q32.3;q24.1) in a Burkitt lymphoma cell line defines a new gene (*BCL7A*) with homology to caldesmon. *Blood* **8**, 3124–3134.

[89] Tracey L, Villuendas R, Dotor AM, Spiteri I, Ortiz P, Garcia JF, Peralto JL, Lawler M, and Piris MA (2003). Mycosis fungoides shows concurrent deregulation of multiple genes involved in the TNF signaling pathway: an expression profile study. *Blood* **3**, 1042–1050.

[90] Alizadeh AA, Eisen MB, Davis RE, Ma C, Lossos IS, Rosenwald A, Boldrick JC, Sabet H, Tran T, Yu X, et al. (2000). Distinct types of diffuse large B-cell lymphoma identified by gene expression profiling. *Nature* **6769**, 503–511.

[91] Martinez-Delgado B, Melendez B, Cuadros M, Alvarez J, Castrillo JM, Ruiz De La Parte A, Mollejo M, Bellas C, Diaz R, Lombardia L, et al. (2004). Expression profiling of T-cell lymphomas differentiates peripheral and lymphoblastic lymphomas and defines survival related genes. *Clin Cancer Res* **15**, 4971–4982.

[92] Adesina AM, Nguyen Y, Guanaratne P, Pulliam J, Lopez-Terrada D, Margolin J, and Finegold M (2007). *FOXG1* is overexpressed in hepatoblastoma. *Hum Pathol* **3**, 400–409.

[93] Rodriguez C, Huang LJ, Son JK, McKee A, Xiao Z, and Lodish HF (2001). Functional cloning of the proto-oncogene brain factor-1 (*BF-1*) as a Smad-binding antagonist of transforming growth factor-beta signaling. *J Biol Chem* **32**, 30224–30230.

[94] Yao J, Lai E, and Stifani S (2001). The winged-helix protein brain factor 1 interacts with groucho and hes proteins to repress transcription. *Mol Cell Biol* **6**, 1962–1972.

[95] Seoane J, Le HV, Shen L, Anderson SA, and Massague J (2004). Integration of Smad and forkhead pathways in the control of neuroepithelial and glioblastoma cell proliferation. *Cell* **2**, 211–223.

[96] Shang C, Fu WN, Guo Y, Huang DF, and Sun KL (2007). Study of the SH3-domain GRB2-like 2 gene expression in laryngeal carcinoma. *Chin Med J (Engl)* **5**, 385–388.

[97] Sun XJ, Sun KL, Zheng ZH, Fu WN, Hao DM, Xu HM, and Li XM (2006). Gene expression patterns in gastric cancer. *Zhonghua Yi Xue Yi Chuan Xue Za Zhi* **2**, 142–146.

[98] Wise DO, Krahe R, and Oakley BR (2000). The gamma-tubulin gene family in humans. *Genomics* **2**, 164–170.

[99] Geurts JJ, Wolswijk G, Bo L, van der Valk P, Polman CH, Troost D, and Aronica E (2003). Altered expression patterns of group I and II metabotropic glutamate receptors in multiple sclerosis. *Brain* **126** (Pt 8), 1755–1766.

[100] Laurin N, Misener VL, Crosbie J, Ickowicz A, Pathare T, Roberts W, Malone M, Tannock R, Schachar R, Kennedy JL, et al. (2005). Association of the calcyon gene (*DRD1IP*) with attention deficit/hyperactivity disorder. *Mol Psychiatry* **12**, 1117–1125.

[101] Gonzalez-Gomez P, Bello MJ, Lomas J, Arjona D, Alonso ME, Aminoso C, De Campos JM, Vaquero J, Sarasa JL, Casartelli C, et al. (2003). Epigenetic changes in pilocytic astrocytomas and medulloblastomas. *Int J Mol Med* **5**, 655–660.

Table W1. Clinical Data for Pediatric PA Patients.

Tumor	Age*	Sex[†]	Location	Survival[‡]
IN1350	4.3	M	Posterior fossa	Unknown
IN1740	8	M	Posterior fossa	160 (A)
IN2110	2.7	M	Posterior fossa	DIS 125 (A)
IN2356	4	M	Cerebellum	142 (A)
IN2368	8	F	Posterior fossa	DIS 87 (A)
IN2524	4	F	Midline-posterior fossa	DIS 39 (A)
IN2604	6	F	Chiasmatic	Unknown
IN2631	4	F	Cerebellum	21 (A)
IN2674	5	M	Cerebellum	112 (A)
IN2788	9	M	Posterior fossa	45 (A)
IN2825	2.75	F	Posterior fossa	104 (A)
IN2921	3	M	Posterior fossa	48 (A)
IN2940	1.75	M	Posterior fossa	74 (A)
IN2969	3.5	F	Posterior fossa	57 (A)
IN3013	11.5	M	Posterior fossa	58 (A)
IN3017	8.25	F	Posterior fossa	59 (A)
IN3115	3.5	F	Optic Pathway	33 (A)
IN3126	9	M	Posterior fossa	31 (A)
IN3156	1.9	M	Posterior fossa	1 (A)

*Age in years at diagnosis.
[†]*F* indicates female; *M*, male.
[‡]Survival in months from date of diagnosis. *A* indicates alive; *DIS*, discharged from hospital.

**Table W2.** Genomic Copy Number RT-QPCR Primer and Probe Sequences and Concentrations.

Locus	Sense 5′–3′	Antisense 5′–3′	Probe 5′–3′	Primer/Probe Concentrations	Fluorescent Label
1p36.32–1p36.33	gaggagttgctctctgcatcct	aacatgccttctgctctggatt	cgcagctcaagagtaga	Sense 300 nM Antisense 900 nM Probe 200 nM	FAM
7q11.23 (*BCL7B*)	gcttacccactgttaggacatgttc	ggcagtatcatgactacggtgatg	tcctaaaccaatcccgc	Sense 300 nM Antisense 900 nM Probe 200 nM	FAM
12q24.33 (*BCL7A*)	aggtgtagaaatgctggttgcat	tttggcacttccctgatatctgt	tgagaagatgtggtccc	Sense 300 nM Antisense 900 nM Probe 200 nM	FAM
14q12	acagaaacggacttggagaagaag	gctcagcgaatggctaattcttt	Accgtctgactgatgaa	Sense 300 nM Antisense 900 nM Probe 200 nM	FAM
FOXG1B (promoter)	tgtggaggacaagttgttcatttg	gctgataacatcttagggccagatt	tgtgttctgcagtattg	Sense 300 nM Antisense 900 nM Probe 200 nM	FAM
β-actin	acgaggcccagagcaagag	gacgatgccgtgctcgat	caccctgaagtaccc	Sense 900 nM Antisense 900 nM Probe 200 nM	VIC

Table W3. MSP Primer Sequences, Annealing Temperatures, and Product Sizes for All Genes Analyzed.

Gene	Sense 5′–3′	Antisense 5′–3′	Annealing Temperature (°C)	PCR Product Size (bp)
CCNA1	(M) tcgtcgcgttttagtcgt	(M) cgttctcccaacaaccg	54.3	200
	(U) gggtagttttgttgtgtttttagtt	(U) ccattctcccaacaaccac	55.1	200
CDKN1C	(M) gggttcgcgcgtataaa	(M) atacgaaaaacgcgacgac	54.7	200
	(U) gggtggggtttgtgtgtat	(U) aaaacacaacaactacctaactatcc	53.7	200
DAPK1	(M) gtcggatcgagttaacgtcg	(M) aaacgccgaccccaaa	56.9	70
	(U) gtttgtgagtgagtgtttagtttg	(U) tctaattacctaaaaccaaattcatca	57.6	70
PRDM2	(M) cgacggcgtagggttaagg	(M) ctatttcgccgaccccg	58.7	150
	(U) ggtgatggtgtagggttaagggt	(U) cactatttcaccaaccccaaca	58.7	150
REPRIMO	(M) tgcgagtgagcgtttagttc	(M) ttacctaaaaccgaattcatc	55.1	100
	(U) gtttgtgagtgagtgtttagttgg	(U) tctaattacctaaaaccaaattcatca	55.7	100
SPINT2	(M) cgagaaggtcgggcg	(M) caaccgttaaaatctcgcg	55.7	150
	(U) gttgagaaggttgggtgtttt	(U) caccaaccattaaaatctcac	54.3	150

Table W4. Sequencing Primers, Annealing Temperatures, and Product Sizes for All Genes Analyzed.

Gene	Sense 5′–3′	Antisense 5′–3′	Annealing Temperature (°C)	PCR Product Size (bp)
CCNA1	(Set1) ggggaagattttttgtggg	(Set1) tcaaacccctaaaaacccaac	56	525
	(Set2) tatagttggagttggagggt	(Set2) caaaacctacctaaaccc	54	490
CDKN1C	(Set1) gtggtgttgttgaaattga	(Set1) cactaatactaaaaaaatcccac	49	420
	(Set2) gtgggatttttttagtattagtg	(Set2) accaaaacactaaacaactactc	49	375
DAPK1	(Set1) ggaaggtagggatttaaaaa	(Set1) accaataaaaaccctacaaac	49	380
	(Set2) gtttgtagggtttttattggt	(Set2) ccttaaccttcccaattact	49	450
	(Set3) gagtaattgggaaggttaagg	(Set3) tcactaaaaacaatctctctcca	52.5	380
PRDM2	(Set1) tgggaatagtaagtttttaaggg	(Set1) caataaccaccacccaacc	55	420
	(Set2) ggttgggtggtggttatt	(Set2) aaaaccccaaataacccca	55	600
REPRIMO	(Set1) gggtttgtttttggttaatagtag	(Set1) caaatttacttcacccaatctc	52.5	390
SPINT2	(Set1) aggaaggaatttataggaaagttg	(Set1) ccaaataccaaaaccccc	53.5	575
	(Set2) gggggtttttggtatttgg	(Set2) attctccctactcaaacccc	57	320
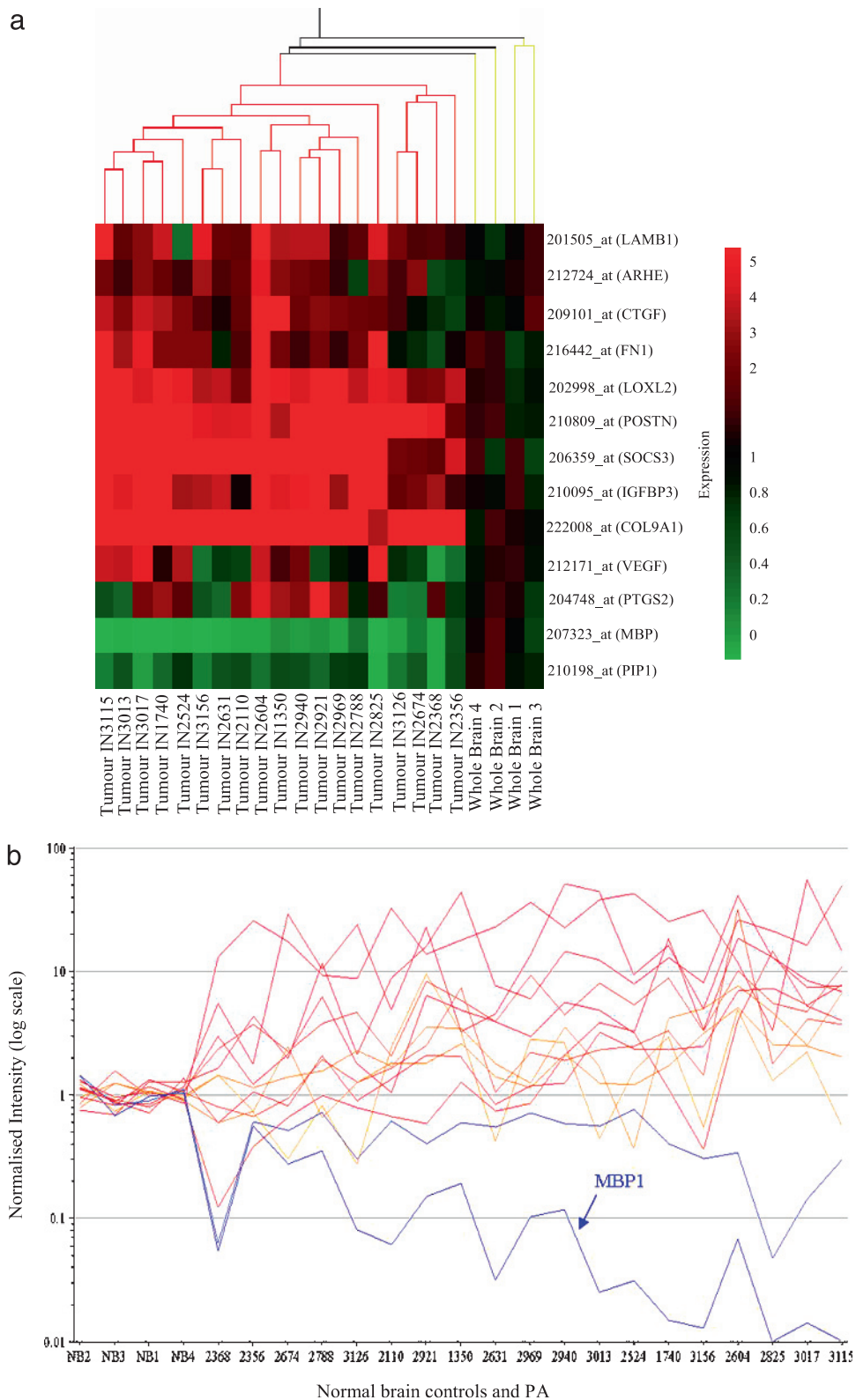
Figure W1. (a) Dendrogram representing the gene expression profile of 13 of 89 genes used by Wong et al. [16] to distinguish possible subgroups in pediatric PA. The dendrogram color saturation is proportional to the magnitude of the difference from the mean, ranging from red (overexpressed) to green (underexpressed). (b) Gene expression profile of 13 of 89 genes used by Wong et al. [16] to distinguish possible subgroups in pediatric PA. The 19 PA are ordered according to expression profile similarity by hierarchical clustering.

Table W6. KEGG Pathways Involved in the Onto-Tools Analysis Approach.

KEGG ID	Pathway Name
1510	Neurodegenerative disorders
4010	MAPK signaling pathway
4020	Calcium signaling pathway
4060	Cytokine–cytokine receptor interaction
4070	Phosphatidylinositol signaling system
4080	Neuroactive ligand–receptor interaction
4110	Cell cycle
4120	Ubiquitin-mediated proteolysis
4130	SNARE interactions in vesicular transport
4140	Regulation of autophagy
4150	mTOR signaling pathway
4210	Apoptosis
4310	Wnt signaling pathway
4330	Notch signaling pathway
4340	Hedgehog signaling pathway
4350	TGFβ signaling pathway
4360	Axon guidance
4370	VEGF signaling pathway
4510	Focal adhesion
4512	ECM–receptor interaction
4514	Cell adhesion molecules (CAMs)
4520	Adherens junction
4530	Tight junction
4540	Gap junction
4610	Complement and coagulation cascades
4612	Antigen processing and presentation
4620	Toll-like receptor signaling pathway
4630	Jak–STAT signaling pathway
4650	Natural killer cell mediated cytotoxicity
4660	T-cell receptor signaling pathway
4662	B-cell receptor signaling pathway
4664	Fc epsilon RI signaling pathway
4670	Leukocyte transendothelial migration
4710	Circadian rhythm
4720	Long-term potentiation
4730	Long-term depression
4740	Olfactory transduction
4742	Taste transduction
4810	Regulation of actin cytoskeleton
4910	Insulin signaling pathway
4912	GnRH signaling pathway
4920	Adipocytokine signaling pathway
4930	Type II diabetes mellitus
4940	Type I diabetes mellitus
4950	Maturity onset diabetes of the young
5010	Alzheimer disease
5020	Parkinson disease
5030	Amyotrophic lateral sclerosis (ALS)
5040	Huntington disease
5050	Dentatorubropallidoluysian atrophy (DRPLA)
5060	Prion disease
5120	Epithelial cell signaling in *Helicobacter pylori* infection
5210	Colorectal cancer

Table W7. RT-QPCR Was Used to Validate Expression Results Generated through Microarray Analysis.

Tumor	TIMP1 Array/RT-QPCR	MCL1 Array/RT-QPCR	SPINT2 Array/RT-QPCR	CCN1A Array/RT-QPCR	MAPK1 Array/RT-QPCR	MATK Array/RT-QPCR
IN1350	10.95/5.46	2.88/1.89	0.24/0.02	0.19/0.00	0.50/0.16	0.04/0.01
IN1740	43.15/35.92	2.281.89	0.18/0.03	0.28/0.00	0.57/0.26	0.03/0.01
IN2110	12.11/9.60	2.33/1.39	0.31/0.03	0.03/0.00	0.43/0.20	0.03/0.01
IN2368	10.20/20.49	5.63/2.34	0.07/0.02	0.17/0.00	0.67/0.29	0.05/0.01
IN2524	13.52/9.54	6.42/1.53	0.24/0.03	0.17/0.00	0.68/0.26	0.03/0.00
IN2604	26.74/20.16	5.25/2.44	0.17/0.02	0.19/0.02	0.85/0.11	0.07/0.00
IN2631	18.05/5.58	6.15/0.78	0.25/0.02	0.32/0.01	0.72/0.17	0.02/0.00
IN2674	7.12/6.26	3.43/1.50	0.57/0.16	0.25/0.02	0.50/0.46	0.03/0.03
IN2825	27.41/32.00	5.43/3.19	0.17/0.03	0.40/0.05	0.46/0.22	0.06/0.01
IN2921	39.89/26.05	3.68/1.16	0.60/0.05	0.14/0.00	0.37/0.13	0.05/0.01
IN2940	17.56/7.78	4.93/1.30	0.28/0.04	0.22/0.00	0.38/0.17	0.03/0.01
IN2969	11.15/9.89	3.57/1.68	0.26/0.05	0.26/0.03	0.48/0.27	0.04/0.01
IN3013	14.69/13.42	3.95/1.33	0.33/0.05	0.14/0.00	0.49/0.17	0.05/0.00
IN3017	13.95/23.92	3.15/3.50	0.13/0.05	0.22/0.01	0.60/0.32	0.04/0.00
IN3126	11.68/11.69	7.56/1.00	0.38/0.08	0.31/0.00	0.67/0.26	0.05/0.01
IN3156	30.88/19.93	3.91/0.89	0.30/0.04	0.26/0.03	0.45/0.18	0.02/0.01

The comparative C_T method was used to determine the relative ratio of expression results for each gene. These were corrected by *β-actin* and referenced to normal brain controls. The relative quantitative value shown previously is expressed as $2^{-\Delta\Delta CT}$.

Table W9. Standard Curve Method (PE Applied Biosystems, Warrington, UK) Used to Calculate the Relative DNA Copy Number of Five Regions of Interest Using *β-actin* as an Endogenous Control.

Tumor	*β-actin**	1p36.32*	Normalized 1p36.33	Copy Number	*BCL7B**	Normalized *BCL7B*	Copy Number	*BCL7A**	Normalized *BCL7A*	Copy Number	14q12*	Normalized 14q12	Copy Number	*FOXG1B* Promoter*	Normalized *FOXG1B*	Copy Number
IN1740	6.70	6.89	1.03	0.54	5.15	0.77	0.38	5.55	0.83	0.53	8.29	1.24	0.71	9.33	1.39	0.50
IN2356	10.90	17.65	1.62	0.85	19.45	1.79	0.88	13.44	1.24	0.79	11.69	1.07	0.62	32.36	2.98	1.07
IN2368	12.58	25.15	2.00	1.05	7.89	0.63	0.31	16.70	1.33	0.85	3.20	1.55	0.89	39.20	3.11	1.12
IN2524	4.53	10.54	2.33	1.22	10.00	2.21	1.08	7.13	1.57	1.01	2.63	0.58	0.33	16.42	3.63	1.30
IN2631	4.48	9.99	2.23	1.17	2.16	0.48	0.24	7.69	1.72	1.10	3.37	1.91	1.10	11.89	2.65	0.95
IN2674	1.32	2.15	1.63	0.85	1.29	0.99	0.48	1.04	0.79	0.51	1.94	1.47	0.85	3.85	2.92	1.04
IN2788	9.79	6.94	0.71	0.37	4.58	0.47	0.23	4.42	0.45	0.29	12.67	1.29	0.74	8.82	0.90	0.32
IN2825	4.47	8.48	1.90	0.99	6.03	1.35	0.66	4.71	1.05	0.67	7.44	1.67	0.96	8.62	1.93	0.69
IN2921	16.87	7.66	1.79	0.93	9.08	2.12	1.03	8.98	0.53	0.34	6.73	1.57	0.90	4.54	1.06	0.38
IN2940	11.12	23.44	2.11	1.10	13.36	1.20	0.59	7.63	0.69	0.44	4.04	1.76	1.01	15.11	1.36	0.49
IN2969	5.38	6.29	1.17	0.61	5.67	1.06	0.52	4.01	0.75	0.48	8.49	1.58	0.91	8.31	1.55	0.55
IN3013	7.68	6.71	0.87	0.46	6.94	0.91	0.44	4.26	0.56	0.35	6.29	0.82	0.47	6.93	0.90	0.32
IN3115	17.70	37.93	2.14	1.12	12.04	0.68	0.33	10.57	0.60	0.38	4.17	1.71	0.98	52.61	2.97	1.06
IN3156	16.47	10.43	0.64	0.33	11.68	0.71	0.35	8.71	0.53	0.34	7.83	0.48	0.28	22.12	1.35	0.48
Controls																
Female	12.75	24.71	1.94	1.02	25.96	2.04	1.00	20.90	1.64	1.05	20.14	1.58	0.91	38.05	2.88	1.03
Male	15.29	28.68	1.88	0.98	31.33	2.05	1.00	23.69	1.55	0.99	28.14	1.84	1.06	40.88	2.68	0.96
IN2886	16.80	30.98	1.84	0.97	33.44	1.99	0.97	25.69	1.53	0.98	31.29	1.86	1.07	45.34	2.70	0.97
IN2827	11.90	23.12	1.94	1.02	24.76	2.08	1.02	19.24	1.62	1.03	21.12	1.77	1.02	31.90	2.68	0.96
IN2766	13.26	24.96	1.88	0.99	26.12	1.97	0.96	20.70	1.56	1.00	21.49	1.62	0.93	38.04	2.87	1.03
IN2887	14.35	28.26	1.97	1.03	30.75	2.14	1.05	21.48	1.50	0.96	25.42	1.77	1.02	42.34	2.95	1.06
Control average			1.91	1.00		2.05	1.00		1.57	1.00		1.74	1.00		2.79	1.00

*Indicates the average nanograms of DNA for the given region generated from the standard curve. The copy number of each region or gene for each tumor is relative to the average control normalized value.
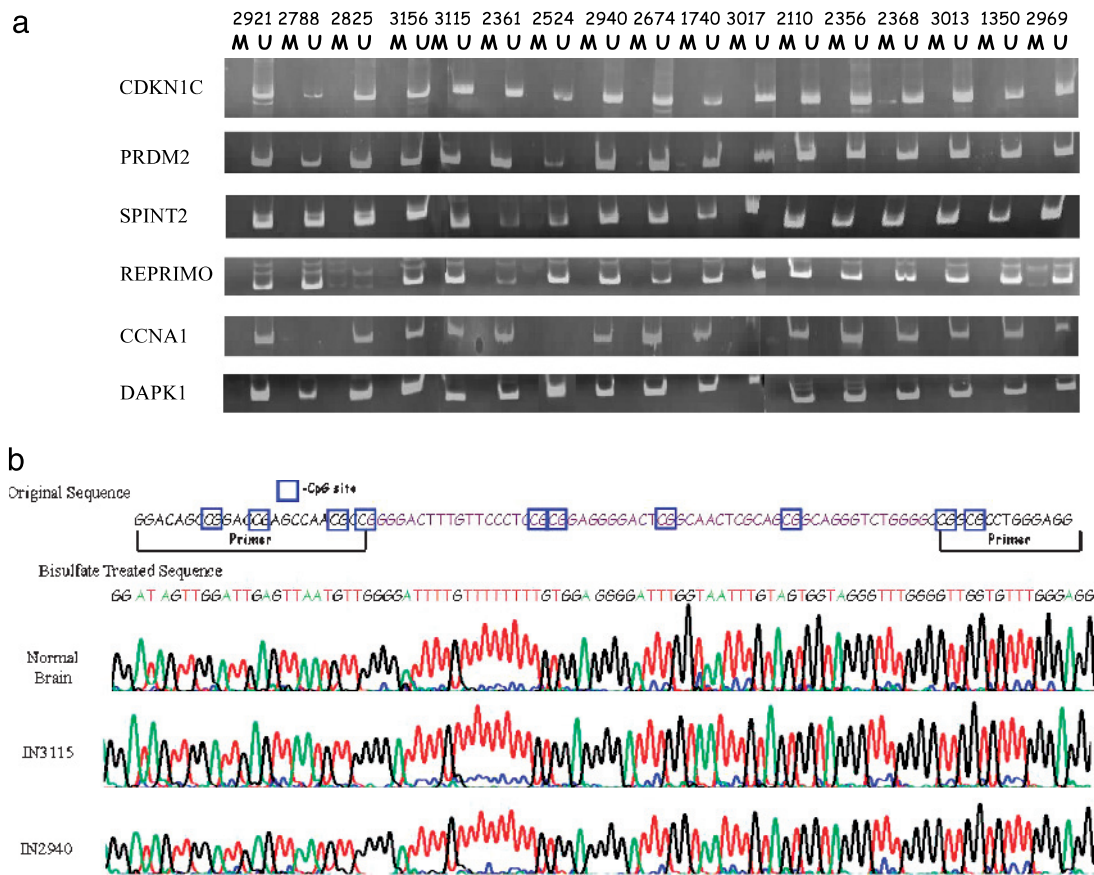
Figure W2. (a) MSP results for *CDKN1C*, *PRDM2*, *SPINT2*, *REPRIMO*, *CCNA1*, and *DAPK1* in pediatric astrocytomas. These results show PCR products for primer sets designed to amplify unmethylated or methylated promoter regions. M indicates methylated products and U indicates unmethylated products for each tumor. (b) Sequencing data for *DAPK1* in PA IN3115 and IN2940 and normal brain. CpG sites where methylation could occur are indicated in the original sequence by a blue box. Unmethylated cytosine residues are converted to uracil residues that, during amplification, become thymidine residues. The bisulfite-treated sequence illustrates no methylation.
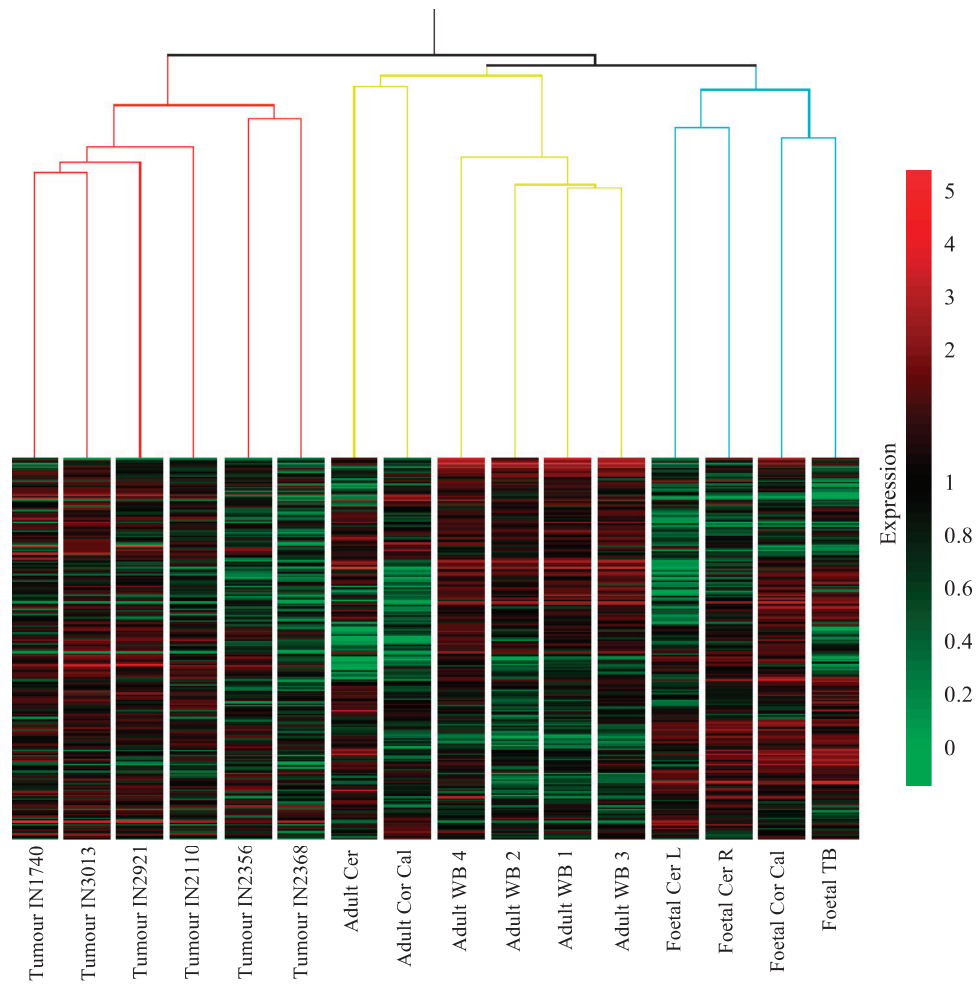
Figure W3. The dendrogram is colored by 7178 genes that were present in all samples and used for this unsupervised hierarchical clustering approach. The samples with red branches are pediatric PA, those with yellow branches are adult normal controls, and those with light blue branches are fetal normal controls. The dendrogram color saturation is proportional to the magnitude of the difference from the experiment median. *Cer* indicates cerebellum; *Cor Cal*, corpus callosum; *WB*, whole brain.